Ultra-Long-Term Delivery of Hydrophilic Drugs Using Injectable *In Situ* Cross-Linked Depots

Sohyung Lee[1,2,3]†, Spencer Zhao[2,3]†, Weihua Jiang[4], Xinyang Chen[2,3], Lingyun Zhu[2,3], John Joseph[1,2,3], Eli Agus[2,3], Helna Baby Mary[2,3], Shumaim Barooj[2,3], Kai Slaughter[2,3], Krisco Cheung[2,3], James N Luo[1,5], Chetan Shukla[2,3], Jingjing Gao[1,2,3,6], Dongtak Lee[1,2,3], Biji Balakrishnan[7], Christopher Jiang[2,3], Amogh Gorantla[2,3], Sukyung Woo[4]*, Jeffrey M Karp[1,2,8,9,10]* and Nitin Joshi[1,2,3]*

[1] Harvard Medical School, Boston, MA, USA

[2] Center for Accelerated Medical Innovation, Department of Anesthesiology, Perioperative and Pain Medicine, Brigham and Women's Hospital, Boston, MA 02115, USA

[3] Center for Nanomedicine, Department of Anesthesiology, Perioperative and Pain Medicine, Brigham and Women's Hospital, Boston, MA, USA

[4] Department of Pharmaceutical Sciences, School of Pharmacy and Pharmaceutical Sciences, The State University of New York at Buffalo, Buffalo, NY 14215, USA

[5] Department of Surgery, Brigham and Women's Hospital, Boston, MA 02115, USA

[6] College of Engineering, University of Massachusetts Amherst, MA, USA

[7] Somaiya Centre for Integrated Science education and research, SKSC, Somaiya Vidyavihar University, Mumbai, 400077, India

[8] Harvard–Massachusetts Institute of Technology Division of Health Sciences and Technology, Massachusetts Institute of Technology, Cambridge, MA 02139, USA

[9] Broad Institute, Cambridge, MA 02142, USA.

[10] Harvard Stem Cell Institute, Cambridge, MA 02138, USA

†Equal contribution

*Corresponding authors: S.W. (skwoo@buffalo.edu) , J.M.K. (jmkarp@bwh.harvard.edu) and N.J. (njoshi@bwh.harvard.edu)

Abstract

Achieving ultra-long-term release of hydrophilic drugs over several months remains a significant challenge for existing long-acting injectables (LAIs). Existing platforms, such as *in situ* forming implants (ISFI), exhibit high burst release due to solvent efflux and microsphere-based approaches lead to rapid drug diffusion due to significant water exchange and large pores. Addressing these challenges, we have developed an injectable platform that, for the first time, achieves ultra-long-term release of hydrophilic drugs for over six months. This system employs a methacrylated ultra-low molecular weight pre-polymer (polycaprolactone) to create *in situ* cross-linked depots (ISCD). The ISCD's solvent-free design and dense mesh network, both attributed to the ultra-low molecular weight of the pre-polymer, effectively minimizes burst release and water influx/efflux. *In vivo* studies in rats demonstrate that ISCD outperforms ISFI by achieving lower burst release and prolonged drug release. We demonstrated the versatility of ISCD by showcasing ultra-long-term delivery of several hydrophilic drugs, including antiretrovirals (tenofovir alafenamide, emtricitabine, abacavir, and lamivudine), antibiotics (vancomycin and amoxicillin) and an opioid antagonist naltrexone. Additionally, ISCD achieved ultra-long-term release of the hydrophobic drug tacrolimus and enabled co-delivery of hydrophilic drug combinations encapsulated in a single depot. We also identified design parameters to tailor the polymer network, tuning drug release kinetics and ISCD degradation. Pharmacokinetic modeling predicted over six months of drug release in humans, significantly surpassing the one-month standard achievable for hydrophilic drugs with existing LAIs. The platform's biodegradability, retrievability, and biocompatibility further underscore its potential for improving treatment adherence in chronic conditions.

Introduction

Patient adherence to medications is a major obstacle to achieving effective treatment of numerous diseases, especially for chronic conditions that require treatment throughout life.[1-3] Long-acting injectables (LAIs) simplify dosing schedules and enhance treatment regimen adherence[4-11], which is particularly advantageous in low-resource settings with limited healthcare infrastructure.[9, 12-14] Multiple LAIs are in clinical use for the treatment and prevention of different diseases.[15, 16] Conventional LAI approaches such as microparticles,[17] *in situ*-forming implants (ISFI), [12, 18] and wet milled particles[6, 15, 19-21] have been documented to achieve prolonged release of hydrophobic drugs for several months but have poor ability to achieve similar ultra-long-term release of

hydrophilic drugs[18, 22-24]. In the case of ISFI, which typically consists of a hydrophobic polymer, poly(lactic-co-glycolic acid) (PLGA) dissolved in a solvent, the solvent efflux during phase conversion tends to release a significant amount of drug as initial burst, which increases with the hydrophilicity of the drug.[18] Additionally, previously developed LAI approaches, including ISFI and microspheres promote significant influx and efflux of water due to their large pores, leading to fast diffusion of hydrophilic drugs.[12, 17, 18] Wet milling – a commonly employed approach for formulating LAIs[19, 20] requires the drug to be hydrophobic and are fundamentally incompatible with hydrophilic drugs.[6, 15, 21] Although implantable devices have shown success for long-term delivery of both hydrophobic[25] and hydrophilic drugs[9, 14], they require invasive, time-consuming medical procedures for insertion, which may pose significant challenges, particularly in low resource settings and low-middle income countries. Furthermore, invasive placement of implants often lead to a higher incidence of local inflammation compared to injectable alternatives, which typically involve less tissue disruption.[26, 27]

Hydrophilic drugs, which we defined as those with a solubility greater than 0.1 mg/mL, constitute a major fraction of all medications used for the prevention, treatment, and management of chronic conditions. Examples include anti-psychotics, anti-depressants, anti-convulsants, antibiotics, and drugs for treating substance abuse disorder (SUD). Although a few hydrophilic drugs have clinically approved LAI formulations, their release typically lasts for only a month. For example, Vivitrol®, an LAI suspension of naltrexone-loaded PLGA microspheres for treating SUD, provides 30 days of drug release,[28] which is sub-optimal since SUD often requires therapy for several years.[29] Therefore, there is an unmet need to develop an injectable platform that enables ultra-long-term delivery of hydrophilic drugs for several months. Additionally, the platform should be designed to be biodegradable for safe breakdown and clearance from the body while also being retrievable in the event of local or systemic drug toxicity.

We report an injectable platform **(Figure 1)** that addresses the limitations of current LAI approaches, enabling ultra-long-term release of hydrophilic drugs for at least 6 months. This platform is derived from an ultra-low-molecular-weight liquid pre-polymer – polycaprolactone (PCL, $500 < M_n < 2000$) , which has been used in multiple FDA-approved products.{Malikmammadov, 2018 #152} PCL is chemically modified with methacrylate groups **(Figure S1A)**, resulting in PCL dimethacrylate (PCLDMA) or PCL trimethacrylate (PCTMA), which can undergo free-radical polymerization in the presence of an appropriate initiator and accelerator. The liquid pre-polymer can

82 effectively suspend or dissolve both hydrophilic and hydrophobic drugs, and can be easily injected through a
83 standard 18-23 gauge needle **(Figure 1A)**. Upon co-injection with a clinically used radical initiator and an
84 accelerator, benzoyl peroxide (BPO) and N,N-dimethylparatoluidine (DMT),[30-32] respectively, the pre-polymer
85 mixture undergoes a time-dependent cross-linking. This process physically encapsulates the drugs, creating a
86 solid structure hereafter referred to as an *in situ* cross-linked depot (ISCD). Hydrolysis of the polymer ester bonds
87 allows gradual erosion of the depot over time, obviating the need for surgical removal after depot exhaustion,
88 and ensuring safe clearance from the body **(Figure S2)**.

89 ISCD has two key features, which enable ultra-long-term release of hydrophilic drugs **(Figure 1B)**. These include
90 a solvent-free design and a dense mesh network, both attributed to the use of ultra-low-molecular weight PCL.
91 The liquid state of the pre-polymer eliminates the need for a solvent, minimizing the risk of high burst release,
92 which is commonly associated with solvent exchange processes in ISFI.[24] Additionally, the ultra-low molecular
93 weight of methacrylated PCL forms a dense mesh upon cross-linking, which limits water influx/efflux, thereby
94 controlling the drug release. We demonstrated that ISCD can exhibit sustained release of multiple hydrophilic
95 drugs with varying water solubilities as high as 100 mg/mL and belonging to diverse therapeutic class, including
96 antiretrovirals, opioid antagonists, and antibiotics. ISCD showed sustained release of all the drugs for at least 6-
97 10 months *in vitro*, suggesting the versatility of the platform. We also demonstrated ultra-long-term release of
98 two proof-of-concept hydrophilic drugs - tenofovir alafenamide (TAF) and naltrexone (NAL) - *in vivo* in rats. A
99 single subcutaneous injection of ISCD formulations loaded with TAF or NAL resulted in sustained plasma
100 concentration for at least 6-7 months. ISCD outperformed the conventional ISFI platform in TAF delivery,
101 exhibiting notably lower burst release compared to ISFI, and providing a prolonged drug release duration of up
102 to 7 months. ISCD also showed ultra-long-term release of a hydrophobic drug – Tacrolimus (TAC) - for at least
103 6 months in rats. Pharmacokinetic (PK) modeling predicted that the ISCD platform can achieve ultra-long-term
104 delivery of naltrexone (NAL) and tacrolimus (TAC) for several months in humans. We also identified design
105 parameters that can tailor the polymer network to tune the drug release kinetics and degradation of ISCD **(Figure
106 1C)**. Notably, modulating intrinsic factors, such as decreasing the concentrations of BPO and DMT or using a
107 higher molecular weight of methacrylated PCL, increases drug release. Additionally, integrating external
108 hydrophilic polymeric additives including polyethylene glycol (PEG) alongside methacrylated PCL can enhance
109 drug release and depot degradation rate, which can be further fine-tuned by varying the degree of methacrylation

110 (mono versus di) of the polymer additive. Finally, we also demonstrated the feasibility of achieving ultra-long-
111 term release of clinically relevant combination regimens of hydrophilic drugs, encapsulated in a single depot,
112 and demonstrated the biocompatibility and retrievability of ISCD.

113 Together, our findings underscore the potential of ISCD as a versatile platform to enable ultra-long-term delivery
114 of both hydrophilic and hydrophobic drugs. To our knowledge, this is the first report demonstrating ultra-long-
115 term delivery (>6 months) of hydrophilic drugs using an injectable system, significantly surpassing the standard
116 of 1-month release avhievable by existing LAI approaches for hydrophilic drugs. This innovation holds the
117 potential to revolutionize therapy options for a variety of chronic conditions where patient adherence is critical.

118 **Results**

119 **Synthesis and characterization of ISCD**

120 The main component of ISCD is ultra-low molecular weight methacrylated PCL ($500 < M_n < 2000$). PCL-diol or -
121 triol were methacrylated *via* a reaction with methacrylic anhydride (MAA) and triethylamine (TEA), resulting in
122 PCLDMA or PCLTMA, respectively **(Figure S1A)**. Methacrylation was confirmed via ^{1}H NMR spectroscopy, with
123 the ratio of integral areas under the protons of the double bond in the methacrylate group at δ = 6.12 ppm (2H,
124 olefinic, cis) to the methylene protons of the PEG segment at δ = 3.70 ppm (4H, -OCH2CH2OCH2CH2O-)
125 determined to be 1:2 **(Figure S1B)**.

126 Upon adding BPO and DMT to PCLDMA or PCLTMA, the pre-polymer mixture undergoes radical polymerization
127 transitioning from a free-flowing liquid solution to a solid monolithic depot. The time interval between the mixing
128 of different components and the complete crosslinking of ISCD is a critical parameter for successful clinical
129 application. Ideally, the crosslinking kinetics should provide sufficient time to mix and inject the formulation before
130 it solidifies. Therefore, we investigated the cross-linking time of ISCD, focusing on the impact of initiator and
131 accelerator concentrations on it. Using a rotational rhemometer, we measured the cross-linking time as the point
132 when the formulation's viscosity starts to rapidly increase. When using 0.1 wt% each of BPO and DMT
133 (BPO/DMT), the formulation demonstrated complete solidification within approximately 9 minutes **(Figure 2A)**.
134 Increasing the concentrations of BPO/DMT from 0.1 to 0.3 wt% significantly reduced the PCLDMA crosslinking

135 time to approximately 5 minutes, which further reduced to 2 minutes with BPO/DMT concentrations of 0.5 wt%.
136 For subsequent experiments, we used 0.3 wt% concentrations of BMO/DMT.

137 Since radical polymerization is an exothermic process, we intended to confirm whether *in situ* crosslinking of
138 ISCD would result in any thermal tissue damage. We employed two complementary techniques: differential
139 scanning calorimetry (DSC) and infrared thermal imaging camera. The DSC analysis showed that the exothermic
140 heat released during the polymerization of PCLDMA increased with increasing concentrations of BPO/DMT.
141 Formulation with 0.5 wt% BMO/DMT showed <4 cal/g exothermic heat release **(Figure 2B)**. To provide context,
142 many common dietary carbohydrates and proteins provide about 4 cal/g of energy.[33] This indicates that the ISCD
143 cross-linking reaction is relatively mild and releases minimal heat. Additionally, monitoring the temperature
144 changes during the polymerization process *via* an infrared thermal imaging camera showed a temperature of
145 20.9 ^{o}C, confirming the absence of localized heating **(Figure S3)**. These findings alleviate concerns about
146 potential thermal tissue damage upon ISCD injection.

147 To assess the ability of ISCD for ultra-long-term release of hydrophilic drugs, we encapsulated TAF – a
148 hydrophilic anti-retroviral with a water solubility of 5.63 mg/mL. We first assessed the injectability of the pre-
149 polymer mixture with and without TAF (90 mg/mL) by determining their viscosities and calculating the injection
150 force using the Hagen-Pouiselle equation[34] under conditions specified in **Figure 2C** for a 23 gauge needle. The
151 calculated injection forces for the pre-polymer mixture with and without TAF were 64.0 ± 3.7 N and 44.4 ± 7.8 N
152 respectively, indicating an increase in viscosity and injection force with drug encapsulation **(Figure 2D,E)**.
153 Importantly, both compositions exhibited injection force values below 80 N, which is considered the maximum
154 acceptable injection force for most people,[34] confirming the injectability of these formulations.

155 *In vitro*, ISCD demonstrated sustained release of TAF, with ~50% cumulative release over 250 days. This was
156 observed for ISCD depots comprising either PCLDMA or PCLTMA **(Figure 2F)**. TAF release kinetics was similar
157 across a range of drug loadings (30-150 mg/mL) **(Figure 2G)**. This indicates that the rate of drug release is
158 independent of the initial amount of drug loaded, but the total amount of drug released ultimately scales
159 proportionally with the initial loading **(Figure S4)**.

160 To function effectively, LAI depots need to maintain their mechanical integrity at the injection site. Therefore, we
161 used a mechanical tester to understand the mechanical properties of ISCD by performing compression testing.

162 ISCD with and without TAF (90 mg/ml) were prepared in a cylindrical mold made of polydimethylsiloxane
163 (PDMS). The compressive stress moduli for ISCDs with and without TAF were 68.1 ± 10.3 MPa and 67.2 ± 4.0
164 MPa, respectively, and the yield stresses were 24.2 ± 1.1 MPa and 25.9 ± 1.5 MPa, respectively **(Figure 2H,I)**.
165 These mechanical properties closely align with those observed in clinically used solid implantable devices[13, 35],
166 confirming the structural rigidity of ISCD. Importantly, the inclusion of TAF does not compromise the structural
167 integrity of the delivery system.

168 We also demonstrated that ISCD can be molded and crosslinked *ex vivo* into various shapes, including cylinders,
169 pipes, and disks, using PDMS molds. These forms maintain a similar drug release profile to the injectable version
170 **(Figure 2J, S5)**, providing a versatile platform for both injectable and implantable drug delivery.

171 **Tailoring the drug release kinetics and degradation of ISCD**

172 Having demonstrated the ultra-long-term release of TAF from ISCD, we aimed to identify design parameters that
173 can tailor the polymer network to fine-tune the drug release kinetics. TAF concentration in ISCD was maintained
174 at 90 mg/ml for all these experiments. We hypothesized that modulating intrinsic factors of ISCD, including the
175 molecular weight of PCLDMA, and the concentrations of BPO and DMT, could influence the cross-linking density
176 of ISCD, thereby impacting drug release. To evaluate the impact of polymer molecular weight on drug release,
177 TAF-loaded ISCDs (90 mg/mL TAF) were formulated using PCLDMA with two distinct molecular weights (630
178 Da and 2100 Da) **(Figure 3A)**. As expected, depots with higher molecular weight polymer showed faster release
179 of TAF. Pevious reports have demonstrated that polymer molecular weight of LAIs impacts crosslinking density,
180 which in turn affects drug release.[36, 37] Similarly, release profiles of TAF from ISCDs with varying concentrations
181 of BPO/DMT ranging between 0.1 to 0.4 wt% demonstrated that an increase in the concentrations of the initiator
182 and accelerator reduces the burst release and the overall release rate **(Figure 3B)**. To confirm if the effect of
183 BMO/DMT concentration on drug release kinetics is attributed to the changes in the cross-linking density of the
184 depot, we quantified the degree of cross-linking of different ISCD depots using a gravimetric approach. The
185 depots were incubated in benzyl alcohol for a week to determine swelling and the Flory-Rehner equation[38] was
186 used to estimate the degree of cross-linking based on the swelling data. As expected, reducing BPO/DMT
187 concentrations resulted in a reduction in the cross-linking density **(Figure 3C)** and an increase in swelling
188 percentage **(Figure S6)**, confirming our hypothesis.

189 Next, we hypothesized that incorporating hydrophilic polymer additives along with PCLDMA would modulate the
190 hydrophilicity of the depot, influencing drug release kinetics. To test this, we added 25 wt% of different polymer
191 additives with varying hydrophilicity but similar molecular weights: polyethylene glycol (PEG, MW 500), PCL-diol
192 (MW 530), and poly(dimethylsiloxane) (PDMS, MW 500). PEG's oxygen-rich polymer chain promotes strong
193 interactions with water, making it highly hydrophilic,[39] while PCL-diol, with hydrocarbon chains and polar ester
194 groups, displays moderate hydrophobicity.[40] PDMS, with its silicone-based structure and methyl-covered
195 surface, is the most hydrophobic among the three polymers.[41] We chose non-methacryalted polymers to ensure
196 that the effects observed on the release kinetics are purely due to the variation in hydrophilicity. Relase profiles
197 of TAF from these ISCDs were compared to the release from unmodified ISCD formulated with pristine PCLDMA.
198 The data support a positive correlation between the hydrophilicity of the additive and the drug release rate from
199 ISCDs. ISCDs containing PEG exhibited the highest cumulative release (46.5 ± 4.5%) at 42 days post-incubation
200 **(Figure 3D, S7)**. This was nearly double the release observed for the unmodified ISCD (24.5 ± 2.3% on day 42).
201 PCL-diol, with intermediate hydrophobicity, also led to a significantly increased release (38.4 ± 2.7%) compared
202 to the unmodified ISCD. Conversely, PDMS, the most hydrophobic additive, showed minimal impact on drug
203 release. These findings suggest that incorporating hydrophilic additives into the polymer network of ISCDs can
204 enhance the drug release rate.

205 Building upon our investigation into the influence of external polymer additives, we sought to explore if
206 methacrylation of the hydrophilic polymer additives and the degree of methacrylation can further impact drug
207 release. To study this, we incorporated 25 wt% of non methacrylated PEG (PEG), singly-methacrylated PEG
208 (polyethylene glycol monomethyl ether mono-methacrylate, PEGMMA), or double-methacrylated PEG
209 (polyethylene glycol dimethacrylate, PEGDMA) along with PCLDMA. All PEG derivatives had the same
210 molecular weight of 500. Increasing the degree of methacrylation reduced both burst release and the overall
211 release rate **(Figure 3E)**. By 240 days, ISCDs with PEG, PEGMMA, and PEGDMA showed cumulative releases
212 of 72.6 ± 5.3 %, 62.5 ± 6.3 %, and 54.2 ± 3.1 %, respectively, which were all significantly higher than the
213 cumulative release of 42.4 ± 5.5 % observed for the unmodified ISCD **(Figure S8A)**.

214 To elucidate the mechanism of increased drug release due to the incorporation of polymer additives, we
215 performed scanning electron microscopy (SEM) based qualitative assessment of depots at week 1 post-

incubation in PBS at 37ºC and also determined their cross-linking density**.** Depot morphology aligned well with the observed drug release behavior **(Figure 3G)**. ISCD containing PEG, the most hydrophilic additive, displayed a highly porous surface compared to the control depot consisting of PCLDMA alone, which showed a densely packed smooth surface. This suggests erosion of PEG-containing ISCD, which could be attributed to the efflux of the uncrosslinked PEG polymer due to its hydrophilicity, leading to enlarged pores, and hence faster drug release than the unmodified ISCD. ISCD with PCL-diol, exhibiting an intermediate hydrophilic character, also showed mild erosion with surface roughness, which explains faster drug release than the unmodified ISCD. Conversely, ISCD with PDMS, the most hydrophobic additive, displayed minimal erosion and a smooth surface, consistent with minimal difference in drug release compared to the unmodified ISCD. Interestingly, PEG-containing ISCD depots also showed significantly lower cross-linking density and swelling percentage compared to the unmodified ISCD **(Figure 3C, S6)**. These observations support the conclusion that incorporating non-crosslinkable hydrophilic polymers as additives can significantly influence the drug release profile from ISCD by decreasing the cross-linking density and promoting erosion of the depot. Notably, unlike non-methacrylated PEG-containing ISCD, SEM images of PEGMMA or PEGDMA-containing ISCD didn't show any signs of depot erosion **(Figure 3G)**, despite their higher TAF release compared to the unmodified ISCD **(Figure 3E)**. However, PEGMMA-containing ISCD showed a significantly lower cross-linking density and higher swelling percentage compared to the unmodified ISCD **(Figure 3C, S6)**. PEGDMA-containing ISCD on the other hand did not show significant changes in cross-linking density or swelling compared to the unmodified ISCD. These findings are consistent with the drug release kinetics, which was significantly faster for PEGMMA-containing depots compared to the ones with PEGDMA, and suggest that the increase in drug release observed with methacrylated hydrophilic polymers is correlated to their ability to reduce the cross-linking density of the network. Significantly increased drug release for PEGDMA-containing ISCD compared to the unmodified ISCD could be attributed to the inherent hydrophilic nature of PEGDMA, which can increase the overall hydrophilicity of the network, thereby increasing water permeability, leading to faster drug diffusion. The absence of depot erosion for PEGMMA and PEGDMA-containing ISCDs can be largely attributed to the ability of PEGMMA and PEGDMA to cross-link within the polymer network. Overall, our data shows that the incorporation of hydrophilic additives in ISCD can enhance drug release by promoting depot erosion, modulating the cross-linking density, or by simply increasing the overall hydrophilicity of the network.

244 The *in vitro* degradation of ISCD was also found to be dependent on the cross-linking density. Degradation was
245 assessed by monitoring mass changes of ISCDs over time while incubated in PBS at 37 °C. After seven months,
246 ISCDs with PEG and PEGMMA exhibited significantly faster degradation, reaching 28.9 ± 2.0% and 19.1 ± 3.0%,
247 respectively, compared to the unmodified ISCD, 12.9 ± 1.3 % **(Figure 3F, S8B)**. In contrast, ISCD with PEGDMA
248 showed a similar degradation profile as the control ISCD, reaching 11.1 ± 2.6 % at 7 months post-incubation, ,
249 which is consistent with their similar cross-linking densities.

250 **Pharmacokinetics and *in vivo* degradation of ISCD**

251 After demonstrating the ultra-long-term release of TAF from ISCD *in vitro*, we aimed to evaluate the
252 pharmacokinetics (PK) of the TAF-loaded ISCD system *in vivo*. Our *in vitro* TAF release data showed faster drug
253 release from PEGMMA-containing ISCD compared to unmodified ISCD. Based on these findings, we selected
254 two ISCD compositions for the *in vivo* study: unmodified ISCD with pristine PCLDMA and ISCD with 25 wt%
255 PEGMMA. Our goal was to confirm if the release tunability observed *in vitro* would also be evident *in vivo*.

256 We subcutaneously injected 500 µL of TAF-loaded ISCDs (90 mg/mL TAF) in rats and used a PLGA-based ISFI
257 formulation as control. It should be noted that TAF is highly unstable in rodent plasma, and rapidly converts to
258 tenofovir (TFV) due to high levels of plasma esterases expressed in rodent species which lead to hydrolytic
259 cleavage of TAF.[14, 43] Because of this reason, we couldn't detect TAF levels in rat plasma, and therefore
260 measured TFV levels to assess the PK. The *in vivo* release rate (µg/day) from ISCD formulations was determined
261 using the area function method[42] by comparing the ISCD PK data (**Figure 3H**) with intravenous (IV) PK data of
262 a single bolus of TAF in rats. Additionally, we performed compartmental PK modeling to quantitatively
263 characterize the *in vivo* PK profiles of ISCDs **(Figures S9-10, Tables 1, S2)**. This involved integrating an
264 appropriate absorption kinetic model describing the *in vivo* release rate of ISCD (**Figure 3I**) with a two-
265 compartment disposition kinetics model describing the IV PK data (**Figure S10A**).

266 Burst release, as characterized by the peak plasma TFV concentration (C_{max}) at 4 hours post-injection was
267 almost 5-fold lower for both unmodified ISCD (133.7 ± 12.7 ng/mL) and PEGMMA-containing ISCD (146.7 ± 27.3
268 ng/mL), as compared to the ISFI formulation (668.0 ± 246.0 ng/mL) **(Figure 3H)**. Following a minimal burst
269 release (<6% of the total drug dose; **Table 1**), plasma TFV levels of rats injected with unmodified ISCDs reached
270 less than 10 ng/mL within 10 days and maintained a sustained level of 1-10 ng/mL for at least 210 days (7

271 months). Based on our PK analysis, the unmodified ISCD maintained a steady daily release rate of 50-100
272 µg/day for at least 7 months **(Figure 3I)**, translating to a cumulative drug release of 81% at 7 months **(Figure**
273 **3J)**. PEGMMA-containing ISCD displayed a distinct release profile compared to unmodified ISCD, characterized
274 by a higher release rate and shorter duration **(Figure 3H-J)**. After a minimal initial burst (<7% of the total dose),
275 plasma TFV levels peaked below 20 ng/mL by day 10 and remained between 10-20 ng/mL until day 63. This
276 was followed by a rapid decline, reaching undetectable levels (<1 ng/mL) after 120 days (4 months). Notably,
277 PCLDMA/PEGMMA released TFV at a significantly higher rate (~200 µg/day) for 2 months compared to
278 PCLDMA **(Figure 3I)**, resulting in a cumulative release of 86% at 3 months **(Figure 3J)**. These PK data are
279 consistent with the trends observed in our *in vitro* release kinetics study. Importantly, both ISCD formulations
280 demonstrated significantly longer sustained release compared to the conventional ISFI system, which exhibited
281 a high initial burst release followed by a rapid decline in plasma TFV levels, falling below the detection limit after
282 2 months.

283 At the end of the study, we retrieved the depots from euthanized rats **(Figure 3K)**, and the remaining drug load
284 was quantified using CHN analysis **(Figure 3L)**. Significantly higher amounts of remaining TAF were observed
285 in the unmodified ISCD compared to PEGMMA-containing ISCD (22.8 ± 3.4% for PCLDMA and 9.1 ± 1.8% for
286 PCLDMA/PEGMMA). Notably, explants from ISFIs at month 2 post-injection exhibited minimal drug remaining
287 (0.26 ± 0.20%) **(Figure S11A)**. ISCDs could be extracted from tissue as a single, easily removable solid depot
288 **(Figure 3K)**, demonstrating superior retrievability, whereas ISFIs were observed as fragile solids, prone to
289 fracture and difficult to extract from the tissue **(Figure S11B)**. We also measured the mass of the remaining
290 depots to assess the biodegradation of ISCD. The remaining mass of the extracted depots was found to be 67.1
291 ± 2.8% for the unmodified ISCD and 45.2 ± 12.1% for PEGMMA-containing ISCD, which correspond to 33% and
292 55% *in vivo* degradation, respectively **(Figure 3M)**. The trend is consistent with the *in vitro* degradation data and
293 confirms that the addition of PEGMMA increases the degradation of ISCD. We also used magnetic resonance
294 imaging (MRI) to evaluate the long-term morphological changes of ISCDs *in vivo* and to study the interactions
295 between depots and host tissues at day 1, month 1, and month 7 after injection **(Figure 3N)**. We confirmed that
296 both unmodified and PEGMMA-containing ISCDs did not migrate to other sites or cause adverse tissue reactions.
297 The size of the depots decreased over time, indicating biodegradation, but both depots maintained good
298 structural integrity. Interestingly, at month 7 post-injection, we found that the PEGMMA-containing ISCD

299 appeared white on MRI images, as did the tissue surrounding the depot, indicating that they had a higher water
300 content than before, while the PCLDMA-only depots remained dark. Since PEGMMA is hydrophilic, higher water
301 content could be attributed to the penetration of water into the depots, as the polymer network loosened over
302 time.

303 It was critical to confirm if TAF encapsulated within the ISCDs didn't degrade into TFV and maintained its
304 chemical structure prior to release. To address this, we employed high-performance liquid chromatography
305 (HPLC) analysis of explanted depots retrieved at 7 months post-injection. The HPLC data of the dissolved
306 explants exhibited a single peak eluting at the same retention time as the freshly prepared TAF solution **(Figure**
307 **S12)**. This confirms the absence of degradation products within the retrieved depots, indicating that TAF remains
308 stable during the crosslinking process and within the depot under *in vivo* conditions prior to its release.

309 **Biocompatibility and safety of ISCD**

310 *In vivo* biocompatibility is essential for LAIs to minimize adverse reactions and inflammation at the injection site,
311 ensuring patient safety and efficacy.[6, 44] We evaluated the biocompatibility of ISCD consisting of pristine PCLDMA
312 without any drug. Depots were injected on day 0, followed by histological and immunohistochemistry (IHC)
313 analysis of the local tissue explanted at week 1, week 4, and month 7 post-injection. The H&E staining and IHC
314 analysis revealed an initial inflammatory response at week 1, characterized by the presence of immune cells,
315 including CD3-positive T cells and CD68-positive macrophages, around the depot **(Figure 4A-C)**. However, by
316 week 4, there was a substantial decrease in the number of immune cells around the depot **(Figure 4B)**,
317 accompanied by a significant reduction in CD3 and CD68 positive populations **(Figure 4C)**, a trend that persisted
318 at month 7, resulting in negligible immune cells present around the depot. Importantly, the tissue samples
319 exhibited no signs of fibrosis, a major complication associated with implant failure and typically identified by
320 excessive collagen deposition.[45] These findings indicate successful integration of the depot with the surrounding
321 tissue.

322 Although ISCD is biocompatible, the drug delivered *via* ISCD may exhibit adverse effects, necessitating prompt
323 depot retrieval. In such cases, a rapid decrease in plasma drug levels following depot removal would be crucial
324 to mitigate side effects. To confirm this, we subcutaneously administered TAF-loaded ISCD to rats and retrieved
325 the depots two weeks later through a small incision near the injection site on the skin **(Figure 4D)**. Plasma TFV

326 levels were monitored after retrieval. Following the depot removal, plasma TFV concentrations showed an
327 exponential decline, decreasing more than four-fold within a day to less than 10 ng/mL **(Figure 4E)**. By day 10
328 post-retrieval, TFV plasma concentrations had dropped below the limit of detection (1 ng/ml) for two out of three
329 rats, and the plasma level went below detection for all three rats by day 14, confirming the safety of ISCD.

330 **Versatility of ISCD for a wide range of therapeutics and combination therapies**

331 Next, we wanted to understand the versatility of the ISCD platform for delivering a broad spectrum of hydrophilic
332 drugs with water solubilities in the range of 3-112 mg/mL. We chose drugs representing diverse therapeutic
333 classes: antiretrovirals, including emtricitabine (FTC), abacavir (ABC) and lamivudine (LAM), an opiate
334 antagonist, naltrexone (NAL), and antibiotics, including vancomycin (VAN) and amoxicillin (AMX). We also
335 evaluated a hydrophobic drug – tacrolimus – a clinically used immunosuppressant. All drugs were encapsulated
336 at a concentration of 90 mg/mL for direct comparison of the release profiles between different drugs. *In vitro*,
337 ISCD demonstrated ultra-long-term release of all the therapeutics over at least 150-360 days **(Figure 5A).** Our
338 analysis revealed a positive correlation between a drug's hydrophilicity and its cumulative release on day 1.
339 Drugs with higher water solubility (more hydrophilic) showed a higher initial release compared to drugs with lower
340 water solubility **(Figure 5B, Table S1)**. This can be explained by the stronger interaction between hydrophobic
341 drugs and the hydrophobic polymer backbone of PCLDMA. However, ISCD successfully minimized the overall
342 burst release for all the drugs. Even for the drugs with water solubilities as high as 100 mg/mL, such as NAL and
343 FTC, day 1 cumulative release was ~20%, which is significantly lower than the cumulative release reported for
344 hydrophilic drugs from injectable systems developed previously.[46, 47]

345 We also demonstrated the potential of ISCD for co-delivery of combination therapies. We encapsulated two
346 clinically used combination regimens for HIV therapy: Epzicom (FTC and LAM) and Descovy (ABC and TAF).
347 We compared the release kinetics of these drugs from ISCD when encapsulated individually versus in
348 combination. Release profiles of drugs encapsulated individually were almost identical to those drugs
349 encapsulated in combination **(Figure 5C,D)**. This suggests that ISCD can be formulated to co-deliver multiple
350 drugs while maintaining their independent release characteristics, making it a promising platform for long-acting
351 combination therapy.

352 Building on the *in vitro* demonstration of ISCD's versatility, we conducted a PK study to validate the ultra-long-
353 term release of drugs with different water solubilities *in vivo*. We selected two drugs with contrasting water
354 solubilities compared to TAF, which showed ultra-long-term release *in vivo*. These included TAC, which has
355 lower water solubility than TAF, and NAL, a drug with higher water solubility than TAF **(Table S1)**. Rats were
356 subcutaneously injected with 500 µL of PCLDMA ISCDs containing either 45 mg/mL of TAC or 90 mg/mL of NAL.
357 Since our *in vitro* data showed a faster release of NAL compared to TAC, we used a higher concentration of NAL
358 than TAC. Blood samples were collected at intervals up to 6 or 7 months post-injection to analyze whole-blood
359 concentration of TAC and plasma concentration of NAL. Similar to TAF, we performed PK analysis for TAC and
360 NAL-loaded ISCDs by utilizing both non-compartmental and compartmental methods. For compartment
361 modeling of the PK profiles **(Figures S9,10, Table S2)**, we established the disposition kinetics by two-
362 compartmental analysis of PK data obtained from experimental bolus intravenous injection of TAC and NAL in
363 rats. Consistent with the *in vitro* release data, ISCD showed a higher initial burst release for NAL *in vivo* (27%)
364 compared to TAC (5.8%) **(Figure 5G,H, Table 1)**, with C_{max} values of 64.9 ± 13.0 ng/mL and 150.7 ± 80.5 ng/mL
365 for NAL and TAC, respectively. Following the initial burst, the ISCD established sustained drug release. As
366 expected based on the water solubilities of NAL and TAC, the systemic concentration of NAL was maintained
367 within a range of 5-15 ng/mL, while TAC concentrations were lower, ranging from 0.5-1.5 ng/mL. This translated
368 to a cumulative release of approximately 92% for NAL and 35% for TAC in 6 months **(Figure 5G,H)**. These
369 findings demonstrate the versatility of the ISCD platform to enable ultra-long-term release of drugs with a wide
370 range of water solubility. The data also establish a clear relationship between a drug's hydrophilicity and its PK,
371 when delivered using an ISCD system.

372 Convolution analysis was utilized to predict the human PK of NAL- and TAC-loaded ISCDs. Human disposition
373 kinetics information was obtained by the analysis of previously reported human PK data for NAL IV bolus[48] and
374 TAC administered orally[49] **(Table S3)**. These human disposition kinetics were then integrated with the release
375 function derived from the PK analysis of NAL and TAC-loaded ISCDs in rats, assuming simple allometry on
376 release rate constants between species. The predicted human PK profiles for NAL and TAC from ISCDs (**Figure
377 5I-J**) were compared with the PK of their clinically available formulations, including oral TAC[49], oral NAL[48], and
378 an intramuscular (IM) LAI of NAL (Vivitrol®)[50]. Notably, a single dose of NAL-loaded ISCD, when injected at 20
379 mg/kg is predicted to maintain prolonged steady plasma concentrations for at least 6 months, well within the

380 established peak and trough levels observed with once-daily oral doses of NAL tablets at 50 mg **(Figure 5I)**.[51]
381 Compared to Vivitrol®, the projected PK profile of NAL-loaded ISCD showed 4.6-fold lower burst release.[50]
382 Interestingly, while Vivitrol®, with a NAL dose of 380 mg, requires a once-monthly injection, the ISCD, with only
383 ~4 times the dose of NAL compared to Vivitrol®, maintains steady plasma concentrations for at least 6 months,
384 suggesting the potential to improve the dosing schedule from once a month to once every 6 months. Similarly,
385 the predicted PK profile of TAC from 3, 4 and 5 mg/kg TAC-loaded ISCDs showed sustained release for at least
386 6 months **(Figure S13)**, with blood levels maintained within the therapeutic concentration range of twice-daily
387 oral doses of TAC capsules (0.038 mg/kg) for 2-3 months **(Figure 5J)**.[49] Overall, our data clearly suggest that
388 ISCD has the potential to enable ultra-long-term release of both hydrophilic and hydrophobic drugs in humans.

389 **Discussion**

390 We present ISCD, an *in situ* cross-linking, biocompatible, and tunable LAI platform designed for ultra-long-term
391 delivery of hydrophilic therapeutics. ISCD is a versatile platform that demonstrated sustained release of multiple
392 hydrophilic drugs with varying water solubilities as high as 100 mg/mL, and from diverse classes of therapeutics,
393 including antiretrovirals, opioid antagonists, and antibiotics. A single subcutaneous injection of TAF-loaded ISCD
394 in rats resulted in significantly prolonged drug release (>7 months) with lower burst release compared to the
395 conventional ISFI system. Prolonged release in rats was also observed for NAL-loaded ISCD, which translated
396 to a predicted 6-month release duration in humans based on PK modeling. This represents a significant
397 improvement over Vivitrol®, a clinically used LAI for NAL, which requires monthly injections and has a higher
398 initial burst. ISCD also demonstrates ultra-long-term release of TAC- a hydrophobic drug.

399 Hydrophobic drugs have been successfully formulated into LAIs that achieve ultra-long-term release over several
400 months. Examples include the bimonthly LAIs for HIV drugs cabotegravir and rilpivirine (APRETUDE® and
401 CABENUVA®), and the recently approved lenacapavir as once every 6 months (SUNLENCA®). Leuprolide
402 acetate, a synthetic hormone used for various conditions including prostate cancer,is available as a once-every-
403 six-months LAI (Eligard®). In contrast, achieving ultra-long-term delivery of hydrophilic drugs, which constitue a
404 substantial portion of therapeutics, remains a significant challenge with LAIs. Currently available LAIs for
405 hydrophilic drugs offer only limited release duration, up to a month, and often result in high burst release.[22]
406 Examples include Zoladex®, a once-monthly injection of goserelin acetate for prostate cancer; Nutropin® Depot,

407 a once- or twice-monthly injection of somatropin for growth failure; Sublocade®, a monthly buprenorphine
408 injection for substance use disorder (SUD); and Vivitrol®, a monthly naltrexone injection for SUD. Additionally,
409 current LAIs are limited to delivering single drugs and have not demonstrated the capability of co-delivery of
410 multiple drugs, in which is crucial for combination therapies, which are the gold standard for treating conditions
411 like HIV. These limitations in LAI technology present a significant barrier to leveraging the full therapeutic
412 potential of hydrophilic drugs, and research dedicated to developing improved LAI platforms for these drugs has
413 been lacking. To our knowledge, this is the first report demonstrating the ultra-long-term release of hydrophilic
414 drugs, either individually or in combination, using an LAI.

415 Our approach offers several advantages over existing methods for long-term delivery of hydrophilic drugs. ISCD
416 offers simple and minimally invasive administration. While implantable devices have demonstrated ultra-long-
417 term delivery of hydrophilic drugs, they require invasive, time-consuming medical procedures for insertion, which
418 can be challenging, especially in low-resource settings and in low- to middle-income countries.[26, 27] For instance,
419 a nanofluidic implant designed for the ultra-long-term delivery of anti-retroviral drugs, including TAF, necessitates
420 a surgical procedure for implant insertion.[52, 53] This involves making a small incision to create a subcutaneous
421 pocket for the implant, followed by sealing the wound with sutures or surgical adhesive under local anesthesia.
422 In contrast, ISCD requires simple subcutaneous or intramuscular injection of the pre-polymer-drug mixture. The
423 final clinical product could be a simple two-component system consisting of 1) a pre-polymer/drug mixture and
424 2) BPO/DMT mixture. This could be either injected using a double barrel syringe or mixed in a vial a few minutes
425 before the injection and injected usual a regular syringe. Another concern for certain implants, such as the
426 nanofluidic implant described above, is that they are non-biodegradable, and require surgical removal after the
427 drug is fully released. ISCD is degradable, and doesn't require surgical removal. Furthermore, ISCD circumvents
428 the limitations of solvent-based LAI formulations (ISFI) such as Sublocade®, which experience significant initial
429 drug loss due to solvent efflux,[54] thereby minimizing the overall release duration. ISCD is a solvent-free system,
430 attributed to the ultra-low molecular weight of the pre-polymer PCLDMA, which helps minimize the burst release.
431 In our study, we demonstrated that TAF-loaded ISCD exhibited a 10-fold lower initial burst release compared to
432 TAF-loaded ISFI, resulting in a significantly prolonged drug release duration of 7 months with ISCD, compared
433 to the 2-month release observed with ISFI. ISCD also exhibits significantly extended release profile compared
434 to microsphere-based LAI approaches such as Vivitrol®. The porous matrix of microspheres promote significant

435 water influx and efflux, resulting in a rapid drug release and a shorter duration. Our SEM data confirmed that
436 ISCD forms a solid depot with dense polymer network, attributed to the ultra-low molecular weight PCLDMA,
437 which limits the water influx and efflux, resulting in prolonged drug release. Previous studies in rats demonstrated
438 that Vivitrol® at 50 mg/kg provided a one-month release of NAL[28]. In contrast, ISCD significantly extends the
439 release duration to at least six months with only a three times higher dose than that of Vivitrol®. The predicted
440 human PK also showed that ISCD can sustain steady plasma concentrations for at least 6 months, compared to
441 only 1 month, as previously documented for Vivitrol®.[55]. Finally, ISCD exhibits excellent retrievability, as it can
442 be easily explanted as a single solid depot , whereas ISFIs are prone to fragmentation during retrieval, as
443 observed in our study.

444 Our study has several strengths. First, to achieve ultra-long term delivery of hydrophilic drugs, we employed a
445 strategically designed yet simple approach. We utilized an ultra-low molecular weight PCL, a polymer that has
446 been used in several FDA-approved products.[40] The ultra-low molecular weight of PCL enabled ISCD to be
447 solvent-free, while forming a dense hydrophobic matrix that minimizes water influx and efflux. To cross-link the
448 methacrylated pre-polymer, we used BPO/DMT-based radical polymerization, a chemical reaction that has been
449 employed in clinical bone cements for over 50 years.[56] Thus, all components of ISCD, including PCL, BPO and
450 DMT have a well-established history of clinical use. Second, we conducted in-depth studies to identify design
451 parameters that can tailor the polymer network to tune the drug release kinetics and degradation of ISCD. To
452 gain mechanistic understanding of how different external additives control the release kinetics, we performed
453 rigorous analysis of cross-linking density using the Flory-Rehner equation and conducted SEM imaging to
454 understand the contribution of surface morphology to the release kinetics. Third, we performed a comprehensive
455 investigation exploring a wide range of hydrophilic drugs to demonstrate the platform's versatility and understand
456 the impact of drug hydrophilicity on release profiles. We studied the release of seven different hydrophilic drugs
457 and one hydrophobic drug for up to 12 months *in vitro,* and validated the release of two hydrophilic and one
458 hydrophobic drug for up to 7 months *in vivo*. We also demonstrated the potential of ISCD for co-delivery of
459 multiple drugs for combination therapy. Fourth, we validated the PK model-based prediction of cumulative
460 release of TAF from the ISCD by quantifying the total drug remaining in the depot using CHN analysis at the end
461 of the study. The cumulative release predictions suggested 19% and 14% of TAF remaining for unmodified ISCD
462 and PEGMMA-containing ISCD, respectively, which aligned well with the 22% and 9% remaining TAF quantified

463 using CHN analysis. Minor discrepancies likely stem from the inherent limitations of the PK model and variability.
464 Nonetheless, this close correspondence between experimental data and model predictions underscores the
465 accuracy and utility of our PK model in describing drug release from ISCD. Finally, to establish translational
466 feasibility of this platform, we performed human PK predictions for ISCD loaded with NAL and TAC, and
467 demonstrated superior PK profiles and simplified dosing schedules compared to their clinically used formulations.

468 While this study establishes a foundation for the ISCD platform, there are limitations and several additional
469 questions that future research needs to address. First, exploring diverse physicochemical properties of
470 therapeutics beyond hydrophilicity will provide a more comprehensive understanding of ISCD release kinetics.
471 While we found a strong correlation between the hydrophilicity of drugs and their release from ISCD, other factors,
472 such as molecular weight and charge, also likely influence a drug's release profile. Therefore, delving deeper
473 into these interactions will be instrumental in optimizing the ISCD platform to accommodate a wider range of
474 therapeutics. Second, while our *in vitro* data successfully demonstrated extended delivery of drug combinations
475 with a single ISCD injection, future studies should validate this *in vivo*. Although we observed minimal
476 interference between multiple drugs in ISCD, investigating the potential impact of complex biological processes
477 on drug interactions *in vivo* will further elucidate ISCD's performance in a living organism for combination therapy.
478 Third, while human PK predictions for TAC-loaded ISCD indicated sustained drug release for at least six months,
479 blood levels fell below the therapeutic window after 2-3 months. This could be attributed to the strong
480 hydrophobicity of TAC combined with limited water influx/efflux in the ISCD, which can result in an ultra-slow
481 release rate, as also observed from the PK analysis of the rat study. Future studies focusing on developing ISCD
482 depots can leverage the design parameters to fine-tune the release kinetics and degradation of TAC-loaded
483 ISCDs, ensuring blood levels are maintained above the therapeutic window for extended durations. Finally, to
484 fully validate the clinical potential of the ISCD platform, it is essential to conduct PK and efficacy studies using
485 clinically relevant large animal models, such as non-human primates. This will further validate the ISCD platform
486 for rapid clinical adoption.

487 Taken together, our approach represents a paradigm shift in long-acting drug delivery, offering the remarkable
488 capability of sustained release of both hydrophilic and hydrophobic drugs over unprecedented durations. This
489 study also provides critical insights into optimizing drug release kinetics in ISCD and highlights the platform's

490 biocompatibility, retrievability, and ability to co-deliver multiple drugs. The platform promises to revolutionize
491 healthcare by addressing the challenges of chronic diseases where consistent medication adherence is critical
492 for therapeutic efficacy.

493 **Methods**

494 **Synthesis of methacrylated polycaprolactone (PCL)**

495 20 ml of 530 Da PCL-diol (Sigma-Aldrich) was mixed with 200 ml dichloromethane in a sealed nitrogen-filled
496 flask chilled to 0°C. 33.8 mL of TEA (Sigma-Aldrich) was added to the flask using a syringe under stirring at 400
497 rpm, and 36 mL MAA (Sigma-Aldrich) was subsequently added dropwise using a syringe to have three molar
498 eqivalent of TEA and MAA per mol of hydroxy group from PCL-diol.[57] The reaction proceeded for 15 hours under
499 stirring at 0°C. The reaction solvent was then removed under reduced pressure and reconstituted in 200 mL of
500 ethyl acetate. The product was washed three times with each solvent: saturated aqueous sodium bicarbonate,
501 0.1 N hydrochloric acid (HCl), and aqueous brine in sequence. Following the washing steps, the product was
502 dried with anhydrous sodium sulfate, filtered under vacuum, and solvent was removed under reduced pressure.
503 The crude product was run through a pre-manufactured silica column (Teledyne Isco) using five column volumes
504 of a mixture of 90% heptane/ 10% ethyl acetate, followed by five column volumes of pure ethyl acetate. Solvent
505 was removed from the latter five fractions under reduced pressure to yield the purified product, PCLDMA, as a
506 viscous yellow liquid. Substitution and purity were confirmed by ^{1}H NMR.

507 **Preparation of pre-polymer mixture and ISCD depots for *in vitro* and *in vivo* samples**

508 Pre-polymer solution, composed of methacrylated PCL (PCLDMA or PCLTMA) with or without external polymer
509 additives (PEG, PEGMMA, PEGDMA, PCL, or PDMS), was mixed with 0.1-0.5 wt% of polymerization initiator,
510 BPO. Drugs were incorporated into the polymer blend, followed by 15 seconds of ultrasonication to facilitate a
511 homogeneous suspension. To initiate the crosslinking, the polymerization accelerator, DMT, was added in at a
512 conetration of 0.1-0.5 wt % and thoroughly mixed, only after all other components had been added, resulting in
513 the pre-polymer mixture. The mixture was drawn into a syringe and injected either into a sink for *in vitro* studies
514 or subcutaneously into a rat for *in vivo* studies. Additionally, the mixture was pipetted into PDMS molds to create

515 different shapes (cylinders, pipes, discs). The mixture underwent polymerization to form a solid depot within 3-
516 10 minutes after the addition of the accelerator.

517 **Mechanical characterization**

518 ISCD depots without or with TAF were prepared in cylindrical PDMS molds (6.8 mm diameter, 2.8mm height) for
519 compression test. The dimensions of the depots were then measured using a caliper. The ISCD depots were
520 mounted between plates of a mechanical tester (ADMET) and compressive force was applied to the samples at
521 a rate of 1 mm/min. The compressive strain and stress on the samples were measured and the compressive
522 moduli were obtained from the linear region (0.15-0.25 mm/mm strain) in the stress-strain curve. (n = 4)

523 **Rheological characterization**

524 A rheometer (Discovery HR-3, TA Instruments) equipped with a parallel plate with a gap size of 1 mm and a
525 diameter of 20 mm was used to characterize the viscosities of the samples and the injection force or to measure
526 the cross-linking time.
527 To evaluate the injection force, PCLDMA without or with TAF (90 mg/mL) was pipetted onto the rheometer at
528 room temperature and any excess solution was trimmed off with a spatula prior to measurements (n=3). The
529 viscosity of the solution was measured while the shear rate was varied from 2 to 3700 s^{-1}. The force required to
530 inject 1 mL of ISCD solution in 30 seconds was measured indirectly from the viscosities using Hagen-Pouiselle
531 equation[34] as follows. Briefly, dynamic viscosities, μ, of ISCD solutions were measured and put into the equation
532 below, where L is length of needle (15 mm); Q is volumetric flow rate (2 mL/min); D is inner diameter of syringe
533 barrel (8.66 mm); and d is inner diameter of needle (0.337 mm).

534 $$F = \frac{32\mu LQD^2}{d^4}$$

535 Briefly, dynamic viscosities, μ, of ISCD solutions were measured and put into the equation below, where L is
536 length of needle (15 mm); Q is volumetric flow rate (2 mL/min); D is inner diameter of syringe barrel (8.66 mm);
537 and d is inner diameter of needle (0.337 mm).

538 For crosslinking time measurements, PCLDMA was prepared with 0.1, 0.3, and 0.5 wt% BPO and mixed with
539 0.1, 0.3, and 0.5 wt% DMT, respectively. Immediately after mixing, the sample was pipetted onto the rheometer

540 and the viscosity of the solution was monitored at a shear rate of 10 s^{-1} until the solutions were crosslinked (n=3).
541 The time when the solutions started to increase in viscosity was recorded as the cross-linking time.

542 **Exothermic heat analysis**

543 To quantify the exothermic heat generated during ISCD polymerization, 15 mg of PCLDMA was prepared with
544 0.1, 0.3, and 0.5 wt% BPO. The mixture was pipetted onto an aluminum pan and combined with 0.1, 0.3, and
545 0.5 wt% DMT, respectively. Immediately after mixing, the heat flow within the sample was measured for 20
546 minutes at room temperature. The total exothermic heat for the reaction was calculated by integrating the heat
547 flow over time. For qualitative analysis, an infrared thermal imaging camera (Fluke Ti95 9Hz) was used to detect
548 the temperature change in the depot during its polymerization.

549 ***In vitro* release**

550 100 µl of Drug-loaded pre-polymer mixtures were injected into a sink medium. For TAC- and AMX-loaded ISCDs,
551 we used 20% methanol in PBS as the sink medium due to low water solubility of these drugs. For other drugs,
552 PBS was used as the sink. Sink containing ISCD depot was incubated in a shaker incubator at 37°C. To maintain
553 sink conditions and prevent bacterial growth, the release medium was completely removed and replaced with
554 fresh release medium every week. The release medium was collected at pre-determined time points to be
555 analyzed directly or after lyophilization and reconstitution with an appropriate solvent for analysis.

556 *In vitro* cumulative release of TAF was analyzed using NMR. TAF release samples were stored in a -80°C freezer
557 and lyophilized after completely frozen. The remaining powder was reconstituted with 500 µL 0.1 mg/mL maleic
558 acid in deuterium oxide (D_2O), as an internal standard, and loaded into NMR tubes (NORELL). NMR experiments
559 were performed on an Agilent MR 400 MHz automated NMR system equipped with a 5mm AutoX One probe at
560 room temperature. Sixty four scans were conducted for each 1H NMR spectrum recording. MestReNova was
561 used for spectrum analysis. Baseline correction of the recorded spectra was performed manually in the software.
562 The maleic acid alkene peak at approximately 6 ppm was integrated, whereas the ppm range of 8.1-8.3 (adenine
563 protons) was integrated and normalized to the maleic acid peak integration area. A 3-point calibration curve was
564 made in a range of 75-300 µg/mL of TAF in D_2O with 0.1 mg/mL maleic acid. The concentration was plotted

565 against the normalized area of integration. Linear regression was generated and used for all TAF sample
566 quantification.

567 The *in vitro* cumulative release other drugs in this study was determined by HPLC (Agilent 1260 Infinity II) and
568 the cumulative drug release was calculated. Sample analyses were performed on a ZORBAX 300SB-C18
569 column (Agilent, 3.0 x 150 mm, 3.5 μm) at 30°C, and all experiments were performed in triplicate. Samples were
570 injected into the HPLC and chromatographic separation was achieved by gradient elution using different mobile
571 phases and flow rates depending on the therapeutics, as described in **Table S1-S3**.

572 **Scanning electron microscopy (SEM)**

573 Surface and microstructures of ISCD were imaged using SEM. First, pre-polymer mixtures with and without
574 encapsulated drugs were prepared and polymerized in a PBS sink. At week 1 post-incubaiton, the implants were
575 removed from the sink and dried overnight under low pressure. The lyophilized samples were subsequently
576 mounted on an aluminum stub using carbon tape, and sputter coated with 6 nm of platinum (Leica EM ACE600).
577 The coated samples were then imaged with Hitachi S-4700 FE-SEM.

578 ***In vitro* degradation analysis**

579 To evaluate the degradation rate of different ISCDs, a weight loss assay was conducted at designated time
580 intervals (Day1/2/4/7/14/28/30/42/60/80) at 37 °C. Depots were formed by injecting pre-polymer mixture into
581 PBS (sink), followed by incubation in a shaker incubator at 37°C. Different samples were prepared for each time
582 point. Sink was decanted at each pre-determined time point, and depots were subjected to freeze-drying for 24
583 hours to remove any residual sink solution. The weight loss (degradation) was quantified as a percentage
584 according to the equation provided below.

585 $$Degradation\ Rate\ (\%) = \frac{W_0 - W_d}{W_0}$$

586 W_0 is the original weight; W_d is the weight of the samples after degradation.

587 **Crosslinking density analysis**

588 The degree of cross-linking of the depots was measured using an equilibrium swelling method and the Flory-
589 Rehner equation, [38] described as follows, where V_r is the volume fraction of depot in swollen state; V_s is molar

590 volume of the solvent (benzyl alcohol), 103.9 mL/mol; χ is the Flory-Huggins polymer-solvent interaction
591 parameter.

592 $$\text{Crosslink density (mol/cm}^3) = -\frac{1}{2V_s}\frac{\ln(1-V_r)+V_r+\chi V_r^{\,2}}{V_r^{\,1/3}-V_r/2}$$

593 ISCD depots composed of PCLDMA with or without external polymer additives (PEG, PEGMMA, PEGDMA, PCL,
594 or PDMS) with 0.3 wt% BPO/DMT and PCLDMA with 0.15 wt% BPO/DMT were prepared. The depots were
595 incubated in benzyl alcohol for a week. The weight of each depot was measured before and after the incubation.
596 The volume fraction of the depots in the swollen state was calculated from the increase in weight using the
597 density of the solvent and polymer mixtures. The Flory-Huggins polymer-solvent interaction parameter was
598 obtained from literature.[58] The parameters were plugged into the Flory-Rehner equation to determine the cross-
599 linking density of each depot.

600 **Animals**

601 Animal experiments were conducted according to ethical guidelines approved by the Institutional Animal Care
602 and Use Committee (IACUC) of Brigham and Women's Hospital. Experiments were conducted in male Sprague-
603 Dawley rats (6-8 weeks, Charles River Laboratories). Rats were maintained under pathogen-free conditions and
604 randomly assigned to various experiment groups. The group size of animals in experiments was decided based
605 on the minimum number of animals required to attain a statistical significance of $P<0.05$ among different test
606 groups.

607 **Pharmacokinetics studies**

608 PK studies were conducted with either unmodified ISCD or ISCD containing 25% PEGMMA. 0.3% BPO/DMT
609 was used and the depots were loaded with TAF, NAL or TAC. The dosages used were 150 mg/kg for TAF and
610 NAL, and 75 mg/kg for TAC. The drug-loaded pre-polymer mixture (500 μL) was administered subcutaneously
611 with an 18 G needle over the shoulder of anesthetized rats. At pre-determined time points, blood was collected
612 from the tail vein of the rats into EDTA-coated tubes.

613 For TAF and NAL analysis, blood samples were centrifuged at 1200g for 10 minutes at 4°C and the supernatant
614 (plasma) was isolated. The Naltrexone/Nalbuphine Forensic ELISA Kit (Neogen) was used to quantify NAL
615 plasma concentrations according to the manufacturer's instructions. TAF and TFV concentrations in plasma

616 samples were analyzed at the PPD Analytical Laboratory (PPD, Inc., Richmond, VA). A 25-μL matrix aliquot is
617 fortified with a TFV-d6 and TAF-d5 internal standard working solution. TFV and TAF are isolated through a
618 protein precipitation extraction. A portion of supernatant is evaporated under a nitrogen stream and the remaining
619 residue is reconstituted. The final extract is analyzed via reversed phase chromatography and MS/MS detection
620 using positive ion electrospray. A linear, 1/concentration² weighted, least-squares regression algorithm is used
621 to quantitate samples.

622 To extract TAC from the blood samples, 100 μL of whole blood was combined with 100 μL of MeOH and 50 μL
623 of 0.1M ZnSO4 in an Eppendorf tube, followed by vortexing. Subsequently, 1 mL of ethyl acetate was added to
624 the mixture and vortexed again. The resulting mixture underwent centrifugation at 14000 rpm for 5 minutes at
625 room temperature. The supernatant was collected and dried, and the measurement of tacrolimus levels was
626 carried out using the Tacrolimus (FK506) ELISA kit (Abbexa, abx515779). The dried TAC sample was
627 reconstituted with the sample diluent buffer provided in the ELISA kit, and further sample analysis was performed
628 following the manufacturer's instructions.

629 **PK analysis and human PK prediction**

630 The PK analysis of ISCD formulations utilized both non-compartmental and compartmental methods. The in vivo
631 release rate (mg/day) from ISCD formulations was determined employing the area function method[41], a
632 deconvolution technique that relies on the relationship between observed drug concentration following
633 subcutaneous injection of ISCD and the area intervals under both subcutaneous and IV drug concentration-time
634 curves. For compartment modeling of ISCD PK profiles in rats, the disposition kinetics of each drug were first
635 established using rat IV PK data obtained experimentally (TFV, TAC) and from literature (NAL)[57-59] with a two-
636 compartment PK model. Subsequently, an appropriate absorption kinetic model was integrated to characterize
637 the ISCD PK profiles. These absorption models describe the in vivo release rate profiles of ISCD, characterized
638 by multiple first-order rates occurring in a sequential manner.

639 For human PK prediction for NAL and TAC following subcutaneous injection of ISCD, convolution analysis was
640 employed, integrating the human disposition kinetic function and the release function of the ISCD formulation.
641 The human disposition function was derived from human IV PK data for TAC[48] and NAL[47] obtained from the
642 literature. The in vivo release functions estimated from the rat PCLDMA ISCD were used after applying simple

643 allometry to release kinetic parameters based on average body size between rats and humans, with a typical
644 allometry exponent of -0.25 for rate constants[60, 61].**Elemental CHN analysis**

645 Residual TAF content within the depots was quantified using elemental analysis (CHN) performed at Midwest
646 Microlab (Indianapolis, IN). Given that the polymer matrix used in the depots lacks nitrogen, the measured
647 nitrogen content can be directly correlated with the remaining amount of TAF. The mass percentages of carbon,
648 hydrogen, and nitrogen in the sample were analyzed, and the residual drug mass within the depots was back-
649 calculated from these values.

650 ***In vivo* degradation**

651 To assess *in vivo* degradation, weight loss of explanted ISCDs was measured. Rats received subcutaneous
652 injections of 500 μL unmodified ISCDs or ISCDs containing 25% PEGMMA (both with 0.3% BPO/DMT but no
653 drugs) (n=3). After 7 months, the rats were euthanized, and the explanted depots were cleared of surrounding
654 tissue. The explants were rinsed with DI water and freeze-dried for 24 hours to remove residual solvents. Weight
655 loss was then calculated as a percentage of degradation using the equation provided below.

656 $$Degradation\ Rate\ (\%) = \frac{W_0 - W_d}{W_0}$$

657 ***In vivo* biocompatibility study**

658 To investigate the inflammatory response caused by the implanted material, rats received injections of either
659 unmodified ISCD or ISCD containing 25% PEGMMA, both formulated with 0.3% BPO/DMT but without any
660 drugs. The depots were explanted at 1 week, 4 weeks, and 7 months post-injection. To assess tissue response
661 over time, histological and immunohistochemical analyses were performed on cryosections of the explanted
662 samples. After explantation, samples were fixed in 4% paraformaldehyde for 4 hours, followed by overnight
663 incubation in 30% sucrose at 4 °C. Samples were then embedded in optimal cutting temperature compound
664 (OCT) and flash frozen in liquid nitrogen. Frozen samples were then sectioned using a Leica Biosystems
665 CM1950 Cryostat. 15-μm cryosections were obtained and mounted in positively charged slides. The slides were
666 then processed for hematoxylin and eosin staining (Sigma) according to instructions from the manufacturer. The
667 stained samples were preserved with DPX mountant medium (Sigma). Immunohistofluorescent staining was
668 performed on mounted cryosections. Anti-CD3 (ab16669) and anti-CD68 (ab125212) (Abcam) were used as

669 primary antibodies, and an Alexa Fluor 594-conjugated secondary antibody (Invitrogen) was used for detection.
670 All sections were counterstained with DAPI (Invitrogen), and visualized on an Leica DMi8 widefield microscope.

671 **Depot retrievability**

672 We subcutaneously administered 500 μL ISCD composed of PCLDMA, 90 mg/mL TAF and 0.3 % BPO/DMT
673 with an 18 G needle to rats and retrieved the depots two weeks later. For the retrieval, the rats were anesthetized
674 and their back was shaved to visualize the location of the depot. Under sterile conditions, a small cutaneous
675 incision was made adjacent to the depot for atraumatic removal using forceps, followed by closure with sterile
676 sutures. Blood (300-500 μL) was collected one hour before retrieval and at day 1, 3, 7, 10, 14, and 21 post-
677 retrieval to monitor plasma TFV levels.

678 **Statistical information**

679 All values are presented as mean ± standard deviation. Two-tailed Student's t-test was used to compare two
680 experimental groups, and one-way ANOVA with Tukey's post hoc analysis was used to compare more than two
681 groups using GraphPad (Software Inc., CA, USA), with P values defined as *< 0.05, **< 0.01, ***< 0.001, and
682 ****< 0.0001. One-way ANOVA with Tukey's post hoc analysis was used to determine the statistical significance
683 of differences in swelling and cross-linking density of ISCD, with the mean of each group compared to the mean
684 of the PCLDMA with 0.3% w/w BPO/DMT (control) group. To compare the *in vivo* plasma TFV level of unmodified
685 ISCD and ISCD containing 25% PEGMMA, we used a two-way ANOVA analysis with time and ISCD formulation
686 as the two variables. One-way ANOVA with Tukey's post hoc analysis was used to determine the statistical
687 significance of differences in residual TAF from explanted depots, with the mean of each group compared to the
688 mean of the unmodified ISCD depot.

689 **Acknolwedgements**

690 We acknowledge funding support from National Institute of Health Grant R21DA057701 (to NJ) and Department
691 of Anesthesiology, Perioperative, and Pain Medicine at the Brigham and Women's Hospital (to NJ and JMK).

692 **Competing interests**

693 S.L., S.Z, J.M.K. and N.J. have one pending patent based on the ISCD formulation described in this manuscript.
694 J.M.K has been a paid consultant and or equity holder for companies (listed here:
695 https://www.karplab.net/team/jeff-karp) including biotechnologies companies such as Stempeutics, Sanofi,
696 Celltex, LifeVaultBio, Takeda, Ligandal, Camden Partners, Stemgent, Biogen, Pancryos, Element Biosciences,
697 Frequency Therapeutics, Corner Therapeutics, Quthero, and Mesoblast. J.M.K. has been a paid consultant and
698 or equity holder for multiple biotechnology companies. The interests of J.M.K. were reviewed and are subject to
699 a management plan overseen by his institution in accordance with its conflict of interest policies.

700 **Author contribution**

701 Conceptualization: SL, SZ, JMK, NJ

702 Methodology: SL, SZ, WJ, BB, SW, NJ

703 Investigation: SL, SZ, WJ, XC, LZ, JJ, EA, HBM, SB, KS, KC, JNL, CS, JG, DL, CJ, AG

704 Supervision: SW, JMK, NJ

705 Writing—original draft: SL, WJ, SW, NJ

706 Writing—review & editing: SL, JMK, NJ

707 **Supplementary Information**

708 Supplementary Information: should be combined and supplied as a separate file, preferably in PDF format.

709 **Reference**

710 1. McLellan, A.T., Lewis, D.C., O'brien, C.P. & Kleber, H.D. Drug dependence, a chronic medical illness:
711 implications for treatment, insurance, and outcomes evaluation. *Jama* **284**, 1689-1695 (2000).
712 2. Sabaté, E. Adherence to long-term therapies: evidence for action. (World Health Organization, 2003).
713 3. Osterberg, L. & Blaschke, T. Adherence to medication. *New England journal of medicine* **353**, 487-497
714 (2005).
715 4. Comer, S.D. et al. Injectable, sustained-release naltrexone for the treatment of opioid dependence: a
716 randomized, placebo-controlled trial. *Archives of general psychiatry* **63**, 210-218 (2006).
717 5. Swindells, S. et al. Long-acting cabotegravir and rilpivirine for maintenance of HIV-1 suppression. *New*
718 *England Journal of Medicine* **382**, 1112-1123 (2020).
719 6. Chaudhary, K., Patel, M.M. & Mehta, P.J. Long-acting injectables: current perspectives and future
720 promise. *Critical Reviews™ in Therapeutic Drug Carrier Systems* **36** (2019).
721 7. Gigante, A.D., Lafer, B. & Yatham, L.N. Long-acting injectable antipsychotics for the maintenance
722 treatment of bipolar disorder. *CNS drugs* **26**, 403-420 (2012).

8. Heres, S., Kraemer, S., Bergstrom, R.F. & Detke, H.C. Pharmacokinetics of olanzapine long-acting injection: the clinical perspective. *International clinical psychopharmacology* **29**, 299 (2014).
9. Li, L. et al. Long-acting biodegradable implant for sustained delivery of antiretrovirals (ARVs) and hormones. *Journal of Controlled Release* **340**, 188-199 (2021).
10. Pacchiarotti, I. et al. Long-acting injectable antipsychotics (LAIs) for maintenance treatment of bipolar and schizoaffective disorders: A systematic review. *European Neuropsychopharmacology* **29**, 457-470 (2019).
11. Shah, A., Xie, L., Kariburyo, F., Zhang, Q. & Gore, M. Treatment patterns, healthcare resource utilization and costs among schizophrenia patients treated with long-acting injectable versus oral antipsychotics. *Advances in Therapy* **35**, 1994-2014 (2018).
12. Maturavongsadit, P. et al. Biodegradable polymeric solid implants for ultra-long-acting delivery of single or multiple antiretroviral drugs. *International Journal of Pharmaceutics* **605**, 120844 (2021).
13. Stewart, S.A. et al. Development of a biodegradable subcutaneous implant for prolonged drug delivery using 3D printing. *Pharmaceutics* **12**, 105 (2020).
14. Gunawardana, M. et al. Fundamental aspects of long-acting tenofovir alafenamide delivery from subdermal implants for HIV prophylaxis. *Scientific reports* **12**, 8224 (2022).
15. Li, W. et al. Clinical translation of long-acting drug delivery formulations. *Nature Reviews Materials* **7**, 406-420 (2022).
16. Nkanga, C.I. et al. Clinically established biodegradable long acting injectables: an industry perspective. *Advanced drug delivery reviews* **167**, 19-46 (2020).
17. Town, A.R. et al. Tuning HIV drug release from a nanogel-based in situ forming implant by changing nanogel size. *Journal of materials chemistry B* **7**, 373-383 (2019).
18. Joiner, J.B. et al. Effects of drug physicochemical properties on in-situ forming implant polymer degradation and drug release kinetics. *Pharmaceutics* **14**, 1188 (2022).
19. Bhakay, A., Merwade, M., Bilgili, E. & Dave, R.N. Novel aspects of wet milling for the production of microsuspensions and nanosuspensions of poorly water-soluble drugs. *Drug development and industrial pharmacy* **37**, 963-976 (2011).
20. Loh, Z.H., Samanta, A.K. & Heng, P.W.S. Overview of milling techniques for improving the solubility of poorly water-soluble drugs. *Asian journal of pharmaceutical sciences* **10**, 255-274 (2015).
21. Wright, J.C. & Burgess, D.J. Long acting injections and implants. (Springer, 2012).
22. Goonoo, N. et al. Naltrexone: A review of existing sustained drug delivery systems and emerging nano-based systems. *Journal of Controlled Release* **183**, 154-166 (2014).
23. Benhabbour, S.R. et al. Ultra-long-acting tunable biodegradable and removable controlled release implants for drug delivery. *Nature communications* **10**, 4324 (2019).
24. Kempe, S. & Mäder, K. In situ forming implants—an attractive formulation principle for parenteral depot formulations. *Journal of controlled release* **161**, 668-679 (2012).
25. Sitruk-Ware, R. New progestagens for contraceptive use. *Human reproduction update* **12**, 169-178 (2006).
26. Kastellorizios, M., Tipnis, N. & Burgess, D.J. Foreign body reaction to subcutaneous implants. *Immune Responses to Biosurfaces: Mechanisms and Therapeutic Interventions*, 93-108 (2015).
27. Su, J.T. et al. A subcutaneous implant of tenofovir alafenamide fumarate causes local inflammation and tissue necrosis in rabbits and macaques. *Antimicrobial agents and chemotherapy* **64**, 10.1128/aac. 01893-01819 (2020).
28. Bartus, R.T. et al. Vivitrex®, an injectable, extended-release formulation of naltrexone, provides pharmacokinetic and pharmacodynamic evidence of efficacy for 1 month in rats. *Neuropsychopharmacology* **28**, 1973-1982 (2003).
29. Koob, G.F. & Volkow, N.D. Neurocircuitry of addiction. *Neuropsychopharmacology* **35**, 217-238 (2010).
30. Zoller, A., Gigmes, D. & Guillaneuf, Y. Simulation of radical polymerization of methyl methacrylate at room temperature using a tertiary amine/BPO initiating system. *Polymer Chemistry* **6**, 5719-5727 (2015).
31. Kim, K. et al. Rational Design of Efficient Amine Reductant Initiators for Amine–Peroxide Redox Polymerization. *Journal of the American Chemical Society* **141**, 6279-6291 (2019).
32. Ramanathan, S. et al. Poly (methyl methacrylate) in Orthopedics: Strategies, Challenges, and Prospects in Bone Tissue Engineering. *Polymers* **16**, 367 (2024).
33. Kwon, Y.-J., Lee, H.S., Park, J.-Y. & Lee, J.-W. Associating intake proportion of carbohydrate, fat, and protein with all-cause mortality in Korean adults. *Nutrients* **12**, 3208 (2020).

34. Watt, R.P., Khatri, H. & Dibble, A.R. Injectability as a function of viscosity and dosing materials for subcutaneous administration. *International Journal of Pharmaceutics* **554**, 376-386 (2019).
35. Kerin, A., Wisnom, M. & Adams, M. The compressive strength of articular cartilage. *Proceedings of the Institution of Mechanical Engineers, Part H: Journal of Engineering in Medicine* **212**, 273-280 (1998).
36. Wang, L., Venkatraman, S. & Kleiner, L. Drug release from injectable depots: two different in vitro mechanisms. *Journal of controlled release* **99**, 207-216 (2004).
37. Li, J. & Mooney, D.J. Designing hydrogels for controlled drug delivery. *Nature Reviews Materials* **1**, 1-17 (2016).
38. Sedov, I. et al. Influence of the cross-link density on the rate of crystallization of poly (ε-Caprolactone). *Polymers* **10**, 902 (2018).
39. Li, K., Qi, Y., Zhou, Y., Sun, X. & Zhang, Z. Microstructure and properties of poly (ethylene glycol)-segmented polyurethane antifouling coatings after immersion in seawater. *Polymers* **13**, 573 (2021).
40. Malikmammadov, E., Tanir, T.E., Kiziltay, A., Hasirci, V. & Hasirci, N. PCL and PCL-based materials in biomedical applications. *Journal of Biomaterials science, Polymer edition* **29**, 863-893 (2018).
41. Wolf, M.P., Salieb-Beugelaar, G.B. & Hunziker, P. PDMS with designer functionalities—Properties, modifications strategies, and applications. *Progress in Polymer Science* **83**, 97-134 (2018).
42. Cheng, H., Staubus, A.E. & Shum, L. An area function method for estimating the apparent absorption rate constant. *Pharmaceutical Research* **5**, 57-60 (1988).
43. Parsons, T.L., Gwenden, K.N. & Marzinke, M.A. Interspecies Differences in Tenofovir Alafenamide Fumarate Stability in Plasma. *Antimicrobial Agents and Chemotherapy* **64**, 10.1128/aac.00930-00920 (2020).
44. Mi, F.-L., Tan, Y.-C., Liang, H.-F. & Sung, H.-W. In vivo biocompatibility and degradability of a novel injectable-chitosan-based implant. *Biomaterials* **23**, 181-191 (2002).
45. Noskovicova, N., Hinz, B. & Pakshir, P. Implant fibrosis and the underappreciated role of myofibroblasts in the foreign body reaction. *Cells* **10**, 1794 (2021).
46. Nanaki, S. et al. New biodegradable poly (l-lactide)-block-poly (propylene adipate) copolymer microparticles for long-acting injectables of naltrexone drug. *Polymers* **12**, 852 (2020).
47. Krovi, S.A. et al. Injectable long-acting human immunodeficiency virus antiretroviral prodrugs with improved pharmacokinetic profiles. *International journal of pharmaceutics* **552**, 371-377 (2018).
48. Wall, M.E., Brine, D.R. & Perez-Reyes, M. Metabolism and disposition of naltrexone in man after oral and intravenous administration. *Drug metabolism and disposition* **9**, 369-375 (1981).
49. Campagne, O., Mager, D.E., Brazeau, D., Venuto, R.C. & Tornatore, K.M. Tacrolimus Population Pharmacokinetics and Multiple CYP3A5 Genotypes in Black and White Renal Transplant Recipients. *Journal of clinical pharmacology* **58**, 1184-1195 (2018).
50. Dunbar, J.L. et al. Single- and Multiple-Dose Pharmacokinetics of Long-acting Injectable Naltrexone. *Alcoholism, clinical and experimental research* **30**, 480-490 (2006).
51. Dean, R.L. The preclinical development of Medisorb Naltrexone, a once a month long acting injection, for the treatment of alcohol dependence. *Frontiers in bioscience* **10**, 643-655 (2005).
52. Chua, C.Y.X. et al. Transcutaneously refillable nanofluidic implant achieves sustained level of tenofovir diphosphate for HIV pre-exposure prophylaxis. *Journal of controlled release* **286**, 315-325 (2018).
53. Pons-Faudoa, F.P. et al. Long-acting refillable nanofluidic implant confers protection against SHIV infection in nonhuman primates. *Science translational medicine* **15**, eadg2887 (2023).
54. Kamali, H. et al. The impacts of PLGA/PEG triblock copolymers with variable molecular weights on the sustained release of buprenorphine. *Current drug delivery* **19**, 357-368 (2022).
55. Dean, R.L. Nonclinical pharmacology of VIVITROL®: A monthly injectable naltrexone for the treatment of alcohol dependence. *Opiate Receptors and Antagonists: From Bench to Clinic*, 655-674 (2009).
56. Arora, M., Chan, E.K., Gupta, S. & Diwan, A.D. Polymethylmethacrylate bone cements and additives: A review of the literature. *World journal of orthopedics* **4**, 67 (2013).
57. Field, J., Haycock, J.W., Boissonade, F.M. & Claeyssens, F. A tuneable, photocurable, poly (caprolactone)-based resin for tissue engineering—synthesis, characterisation and use in stereolithography. *Molecules* **26**, 1199 (2021).
58. Barton, A.F. CRC handbook of solubility parameters and other cohesion parameters. (Routledge, 2017).

Figures and figure legends

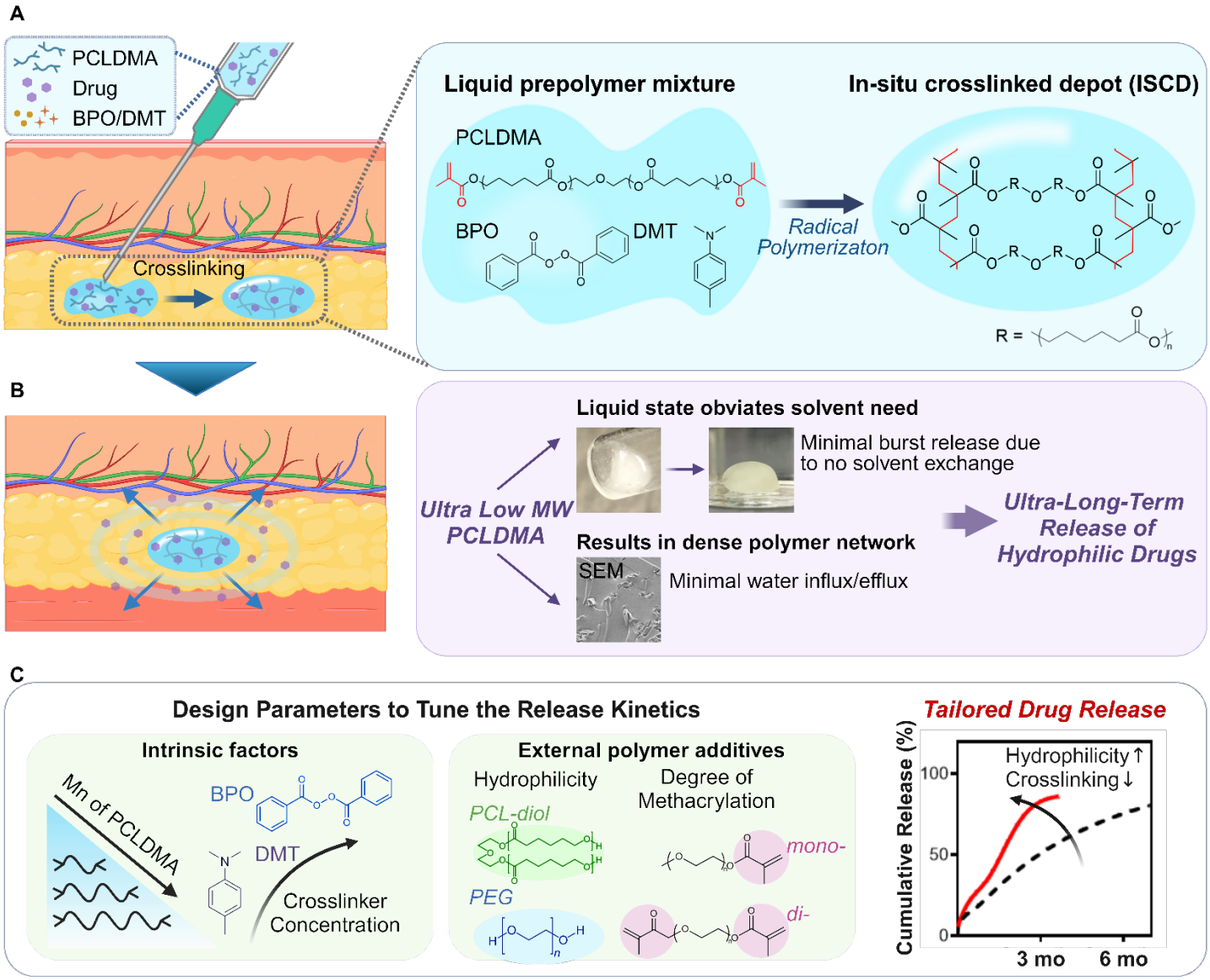

Figure 1. Injectable *in situ* crosslinked depot (ISCD) platform for sustained release of hydrophilic therapeutics. A. The main component of ISCD is low molecular weight liquid methacrylated PCL, for example, PCLDMA. The liquid pre-polymer can suspend or dissolve both hydrophilic and hydrophobic drugs and can be easily injected through a standard 18-23 gauge needle. Upon adding an initiator (BPO) and accelerator (DMT) to PCLDMA, the pre-polymer mixture undergoes radical polymerization transitioning from a free-flowing liquid solution to a solid monolithic depot, resulting in physical encapsulation of the drug. **B.** ISCD has two key features enabling ultra-long-term release of hydrophilic drugs: a solvent-free design and a dense mesh network, both attributed to the ultra-low-molecular weight of the pre-polymer, PCLDMA. The liquid state of the pre-polymer

841 obviates the need for a solvent, minimizing burst release. Cross-linking of the ultra-small chains of the pre-
842 polymer results in a dense network (as shown in the SEM image of an ISCD depot formed *in vitro*) that limits
843 water influx and efflux, minimizing the drug release rate. **C.** Design parameters to tailor the ISCD network to tune
844 the drug release kinetics. Modulating the intrinsic factors, including decreasing the concentrations of BPO and
845 DMT, or using higher molecular weight PCLDMA increases drug release. Additionally, adding external polymer
846 additives including polyethylene glycol (PEG) and PCL-diol alongside PCLDMA can enhance the depot's
847 hydrophilicity, increasing drug release. External additives with different degrees of methacrylation (mono or di)
848 can further tune the drug release. The cumulative release profiles of TAF from two different ISCD depots injected
849 subcutaneously into rats are shown as examples of tailored drug release with varying release rates. Lowering
850 the crosslinking density and increasing the hydrophilicity of the polymer chains achieve faster drug release.
851
852
853
854
855
856
857
858
859

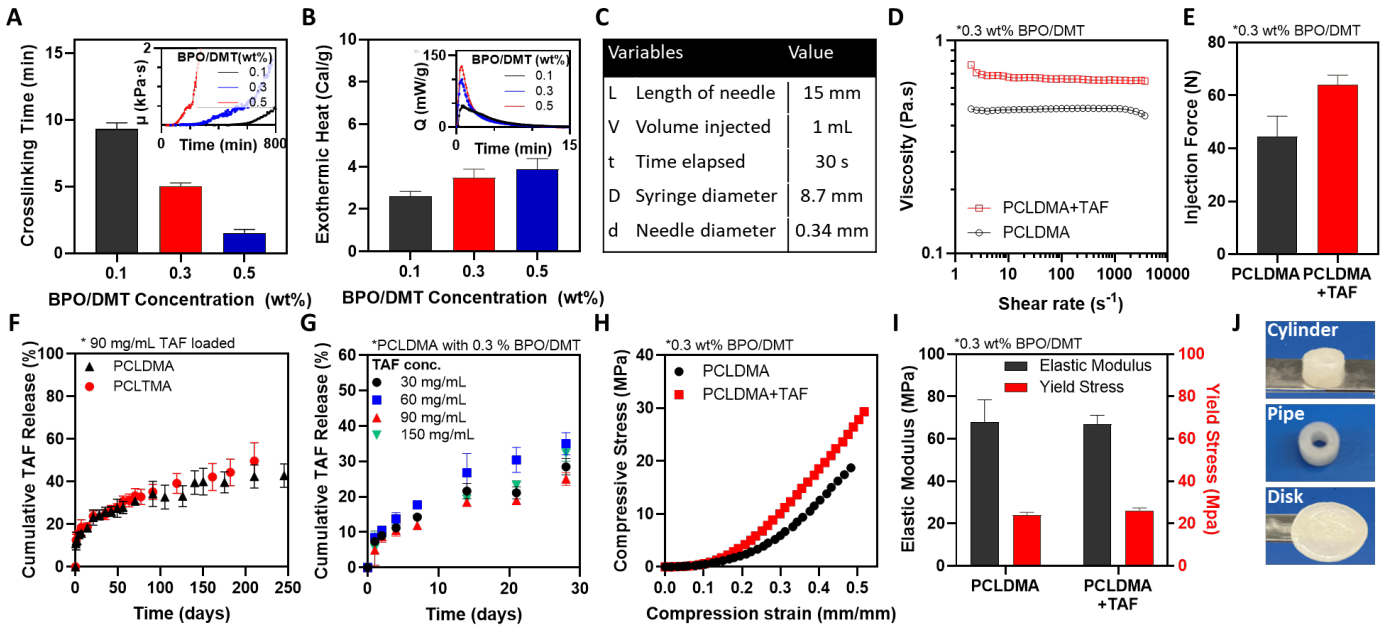

Figure 2. Synthesis and physiochemical characterization of the ISCD platform. A. The cross-linking time for PCLDMA at different BPO/DMT concentrations is shown. Cross-linking time was measured as the point at which the viscosity of the pre-polymer mixture, monitored with a rheometer, begins to increase rapidly, as shown in the inset. **B.** Exothermic heat released during the cross-linking of ISCD with varying concentrations of BPO/DMT, measured using DSC. **C.** Injection parameters for the Hagen-Poiseuille equation used to calculate the injection force for PCLDMA, with or without TAF, using a 23-gauge needle. **D.** Viscosities of PCLDMA, with or without TAF, measured using a rheometer. **E.** Injection force calculated for PCLDMA, with or without TAF. The maximum acceptable injection force is 80 N. **F.** *In vitro* release profile of TAF in PBS (37°C) from ISCD comprising either PCLDMA or PCLTMA. **G.** *In vitro* release profile of TAF in PBS (37°C) from ISCD loaded with concentrations of TAF. **H.** Compressive stress-strain curves for ISCD with or without TAF, measured using a mechanical tester. **I.** Elastic moduli and yield stress for ISCD with or without TAF. **J.** ISCD can be polymerized *ex vivo* into various shapes such as cylinders, pipes, or disks that can be used as ultra-long-acting implants. Data in A, B, E-G, and I are presented as mean ± standard deviation (n=3, replicates performed at least twice). Data in D and H are representative of a single experiment (repeated three times).

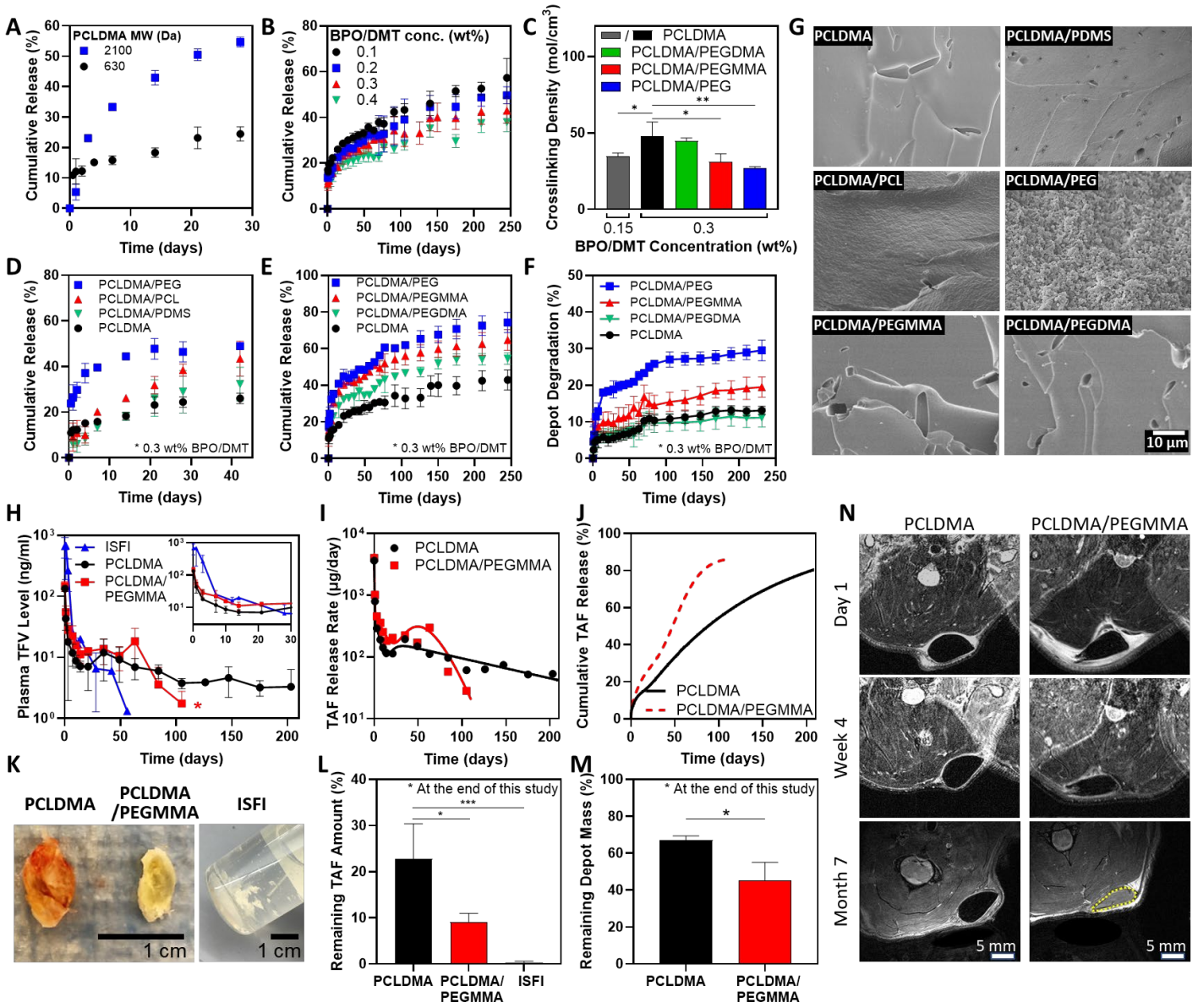

Figure 3. Tailoring the drug release kinetics and degradation of ISCDs *in vitro* and *in vivo*. A. *In vitro* release profiles of TAF in PBS (37°C) from ISCDs prepared with PCLDMA of different molecular weights (630 Da and 2100 Da). **B.** *In vitro* release profiles of TAF in PBS (37°C) from ISCDs prepared with varying BPO/DMT concentrations. **C.** Crosslinking density of unmodified ISCD prepared with different concentrations of BMP/DMT and ISCD containing different external polymer additives (25 wt%) (*P<0.05 and **P<0.01). **D.** *In vitro* release profiles of TAF in PBS (37°C) from unmodified ISCD (prepared using PCLDMA only) or ISCD containing 25 wt% of an external polymer additive (PEG, PCL, or PDMS) alongside PCLDMA. **E.** *In vitro* release profiles of TAF and **F.** and percentage depot degradation in PBS (37°C) for unmodified ISCD or ISCD containing 25 wt% of PEG with varying degrees of methacrylation. **G.** SEM images of unmodified ISCD or ISCD containing different

888 external polymer additives (25 wt%) showing the cross-section of depot structure at week 1 post-incubation in
889 PBS (37°C). **H.** Plasma level of TFV in rats injected with 500 µl of TAF-loaded ISFI (control) or TAF-loaded
890 unmodified ISCDs of ISCD containing 25 wt% PEGMMA. All depots were loaded with 90 mg/mL of TAF. The
891 inset shows plasma levels up to day 30. (*P<0.05 for the overall comparison of plasma levels of the two ISCDs
892 over the entire study duration). **I.** *In vivo* daily release rate and **J.** cumulative release of TAF from unmodified
893 ISCD or ISCD containing 25 wt% of PEGMMA, as determined by PK modeling. **K.** Camera images of TAF-
894 loaded ISFI or TAF-loaded unmodified ISCD or ISCD containing 25 wt% of PEGMMA, retrieved from rats at
895 month 7 post-injection, and **L.** Remaining TAF amount in the depots (*P<0.05 and ***P<0.001) and **M.**
896 Remaining mass of the depot (*P<0.05). Due to the disintegration of ISFI within the animal, the remaining mass
897 of the ISFI depots could not be measured. **N.** MRI images of subcutaneously injected unmodified ISCD or ISCD
898 containing 25 wt% PEGMMA at different time points. Data in A, B, C, E, F, and G are presented as
899 mean ± standard deviation (n=3, experiments performed at least twice). Data in H, L, and M are presented as
900 mean ± standard deviation of technical repeats (n=3, experiment performed twice). Data in I and J present
901 predictions from PK modeling of the average plasma levels of TFV obtained experimentally. *P*-value in H was
902 determined using two-way ANOVA with Bonferroni correction, with time and different ISCD formulations as the
903 two variables. The *P*-value in C and L was determined using one-way ANOVA with Tukey's post hoc analysis.
904 The *P*-value in M was determined using Student's *t*-test.

905

906

907

908

909

910

911

912

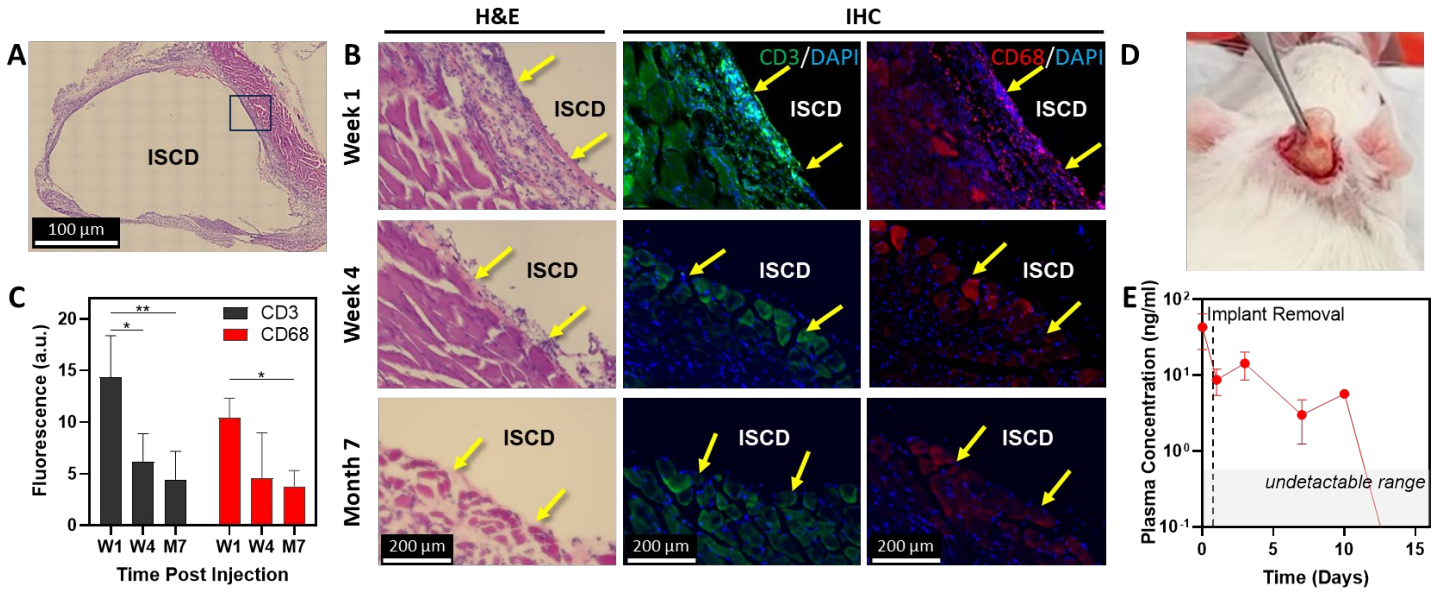

Figure 4. *In vivo* biocompatibility and safety of ISCD. A. Representative image (10X magnification) of an H&E stained section of local tissue, explanted with the ISCD depot one week after subcutaneous injection of 500 µl PCLDMA-based ISCD in rats. **B.** Left side shows high magnification (20X) representative images of H&E-stained sections of local tissue, explanted with the ISCD depot at different time points. Yellow arrows show inflammatory cells. The right side shows representative immunofluorescence images of local tissue sections explanted at different time points and stained against CD3 (green) and CD68 (red) markers to visualize T cells and macrophages, respectively. Yellow arrows show cells positive for CD3 or CD68. **C.** Fluorescence intensity quantified for CD3 and CD68 immunofluorescence. (*P<0.05, **P<0.01). **D.** Camera image taken during the procedure of retrieving ISCD from a rat, showing safe retrievability *via* a small incision. **E.** Plasma levels of TFV following ISCD removal. Data in C and E are presented as mean ± standard deviation of technical repeats (n=3). The *P*-value in C was determined using one-way ANOVA with Tukey's post hoc analysis.

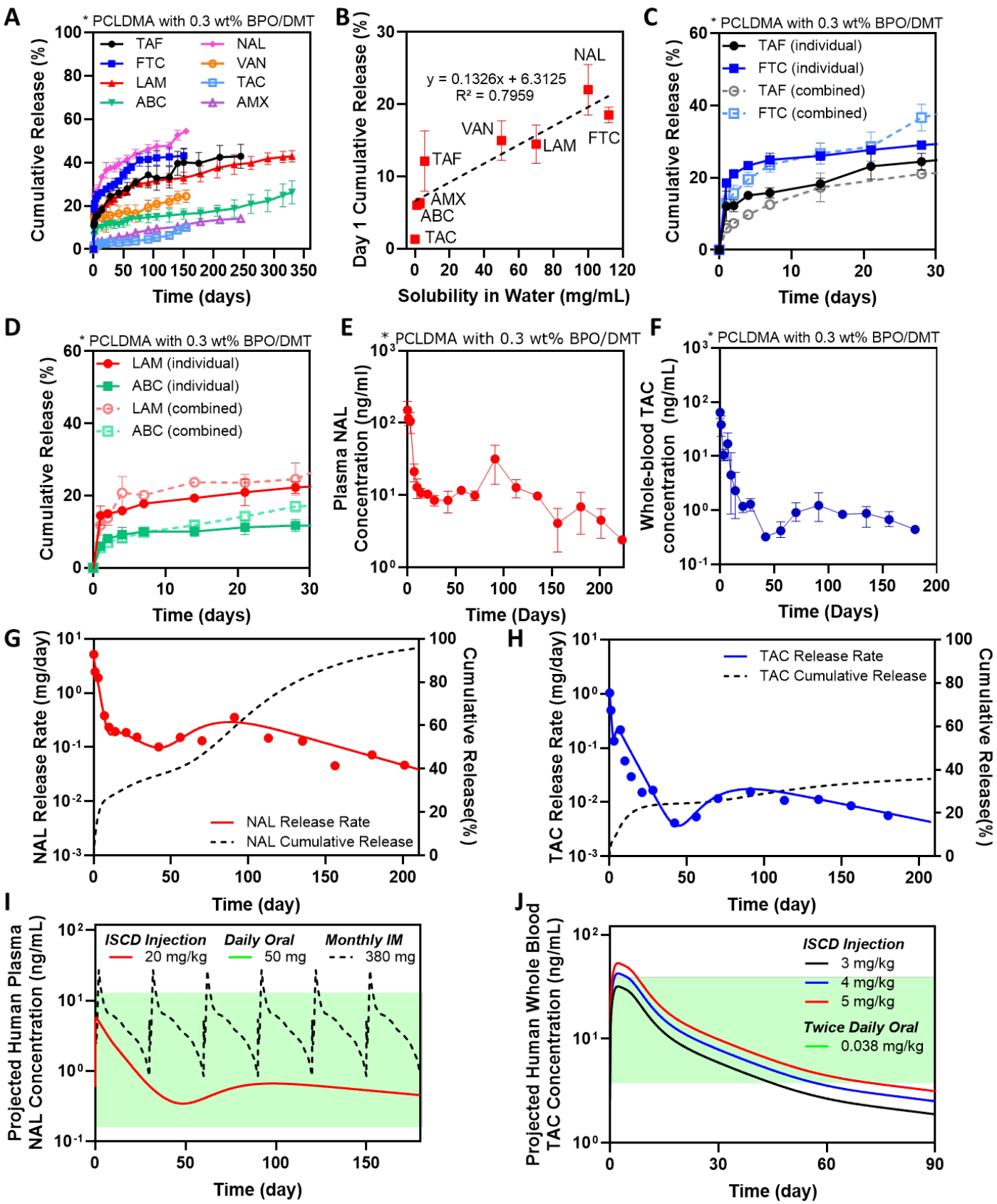

930

931 **Figure 5. The versatility of the ISCD platform and human PK prediction. A.** *In vitro* release profile of different

932 drugs with varying water solubilities encapsulated into the ISCD platform. The release was studied in PBS (37°C).

933 **B.** Correlation of cumulative release at day 1 with different drugs with varying water. **C.** *In vitro* release profile of
934 TAF and FTC, when loaded into the ISCD platform individually versus in combination. The release was studied
935 in PBS (37°C). **D.** *In vitro* release profile of ABC and LAM, when loaded into the ISCD platform individually versus
936 in combination. The release was studied in PBS (37°C). **E.** Plasma concentration of NAL in rats subcutaneously
937 injected with 500 µl of NAL-loaded ISCD (45 mg/ml NAL). **F.** Whole blood concentration of TAC in rats
938 subcutaneously injected with 500 µl of TAC-loaded ISCD (28 mg/ml TAC). *In vivo* daily release rate and
939 cumulative release profile of **G.** NAL and **H.** TAC, as predicted by PK modeling of systemic drug levels in rats,
940 following subcutaneous injection of 500 µl of NAL- or TAC-loaded ISCD. **I.** Convolution analysis-based prediction
941 of human PK of a single subcutaneous dose of NAL-loaded ISCD in comparison to clinically established PK
942 profile of once-daily oral dose of NAL (green region), and once monthly intra-muscular injection – Vivitrol®
943 (purple lines). **J.** Convolution analysis-based prediction of human PK of a single subcutaneous dose of TAC-
944 loaded ISCD (at different dosages) in comparison to clinically established PK profile of twice-daily oral doses of
945 TAC (green region). Data in A-D are presented as mean ± standard deviation (n=3, experiments performed at
946 least twice). Data in E and F are presented as mean ± standard deviation of technical repeats (n=3). Data in G
947 and H present predictions from PK modeling of the average plasma level of TAC and NAL obtained
948 experimentally. Data in I and J present human PK prediction based on convolution analysis of experimentally
949 obtained PK data of TAC and NAL in rats.

950

951

952

953

954

955

956

957

958 **Tables**

959 **Table 1.** Drug release kinetic parameters for drug-loaded ISCD formulations.

Drug Release phase	TAF-loaded PCLDMA ISCD			TAF-loaded PCLDMA/PEGMMA ISCD		
	Rate constant (1/day)	Cumulative release (%)	Time delay (day)	Rate constant (1/day)	Cumulative release (%)	Time delay (day)
Initial	2.47	5.8		2.52	6.8	
Intermediate	0.178	9.2	1.5	0.0643	27.1	1.0
Sustained	0.00744	65[#]	18.1	0.128	52.1[#]	50.8
Drug Release phase	**TAC-loaded PCLDMA ISCD**			**NAL-loaded PCLDMA ISCD**		
	Rate constant (1/day)	Cumulative release (%)	Time delay (day)	Rate constant (1/day)	Cumulative release (%)	Time delay (day)
Initial	0.962	8.7		0.372	27.4	
Intermediate	0.122	15.6	3.7	0.0346	15.4	11.8
Sustained	0.0134	10.7[#]	68.3	0.0181	54.2[#]	70.1

960 [#]Calculated as %Total drug mass released in vivo by the end of the study -%Release by initial and
961 intermediate phases
962
963